AGU PUBLICATIONS

JGR

Journal of Geophysical Research: Oceans

RESEARCH ARTICLE

10.1002/2015JC010933

Slow westward movement of salinity anomalies across the tropical South Indian Ocean

J. Mauro Vargas-Hernandez[1,2,3], Susan Wijffels[2,4], Gary Meyers[1,2], and Neil J. Holbrook[1,5]

[1]Institute for Marine and Antarctic Studies, University of Tasmania, Hobart, Tasmania, Australia, [2]CSIRO Oceans and Atmosphere Flagship, Hobart, Tasmania, Australia, [3]Laboratorio de Oceanografía y Manejo Costero (LAOCOS), Universidad Nacional, Heredia, Costa Rica, [4]Centre for Australian Weather and Climate Research, Hobart, Tasmania, Australia, [5]ARC Centre of Excellence for Climate System Science, Hobart, Tasmania, Australia

Key Points:
- Decadally varying salinity anomalies move westward in the tropical SIO
- Decadal salinity anomaly originates mostly in the subtropical eastern SIO
- Salinity anomalies are consistent with nonlinear baroclinic disturbances

Correspondence to:
J. M. Vargas-Hernandez,
jose.vargas.hernandez@una.cr

Citation:
Vargas-Hernandez, J. M., S. Wijffels, G. Meyers, and N. J. Holbrook (2015), Slow westward movement of salinity anomalies across the tropical South Indian Ocean, *J. Geophys. Res. Oceans*, *120*, 5436–5456, doi:10.1002/2015JC010933.

Received 22 APR 2015
Accepted 16 JUL 2015
Accepted article online 21 JUL 2015
Published online 6 AUG 2015

Abstract Decadal salinity variability is an important characteristic of the ocean. It characterizes differences in evaporative and precipitation fluxes at the surface, and in the subsurface it contributes to steric sea level change and freshwater/salt transports. In this paper, we identify and describe westward moving and decadally varying salinity anomalies within the thermocline of the tropical South Indian Ocean (SIO) based on ocean state estimates from the Simple Ocean Data Assimilation version 2.2.4 (SODA). This signature in the salinity anomalies is expressed at the depth of 20°C isotherm (D20). A two-dimensional radon transform quantifies the westward speeds as being between 0.4 and 1.7 cm s^{-1}. These speeds are slower than those of first baroclinic-mode Rossby waves or mean advection speeds of the background flow in the same regions. The decadal salinity anomaly originates in the subtropical eastern SIO (∼ 39% of the variance explained) and merges with remote anomalies from the western tropical Pacific Ocean (WTPO) via the Indonesian Seas (∼ 11% of the variance explained). The eastern SIO displays both decadal (∼ 10–15 years) and interdecadal (∼ 15–30 years) variability influenced by the WTPO, whereas the decadal variability in the western SIO seems to be more influenced by signals originating in the subtropical eastern SIO. We conclude that these salinity anomalies are consistent with signatures of nonlinear baroclinic disturbances as explained in the recent literature, and possible interaction of higher order baroclinic-mode Rossby waves with the mean flow.

1. Introduction

While the Indian Ocean displays a near uniform surface multidecadal warming trend [*Alory et al*., 2007; *Alory and Meyers*, 2009], there is also significant subsurface cooling evidenced in sea surface height (SSH) data (as well as in ocean heat content (OHC), thermocline depth and temperature) and expressed as cooling of the thermocline waters of the tropical South Indian Ocean (SIO) [*Han et al*., 2006; *Alory et al*., 2007; *Trenary and Han*, 2008; *Schwarzkopf and Böning*, 2011; *Trenary and Han*, 2013]. While this multidecadal signal appears to be the strongest low-frequency variability in the SIO, there is also evidence of interannual and decadal variability in the dynamics [*Meyers*, 1996; *Wijffels and Meyers*, 2004; *Cai et al*., 2005; *Alory et al*., 2007; *Feng et al*., 2010; *Nidheesh et al*., 2013; *Trenary and Han*, 2013; *Vargas-Hernandez et al*., 2014; *Han et al*., 2014], as well as decadal variability of salinity anomalies within the thermocline of the tropical SIO, which is the focus of the present study.

1.1. Review of Low Frequency Variability in the Indian Ocean

Low-frequency variability studies of the tropical SIO have focused on thermal changes associated with OHC, SSH and subsurface temperature, but little research has been undertaken to understand the decadal variability of salinity anomalies and their contribution to steric SSH. For instance, *Vargas-Hernández* [2014] showed that steric SSH had a positive trend whereas the thermosteric SSH (ThSSH) displayed a negative trend for the period 1970–2003 averaged across a zonal band of the SIO (10.25°S–30.25°S, 30.25°E–120.75°E), pointing to the important role that salinity variability plays in the Indian Ocean. Linear trends of steric sea level for short periods (< 30 years, for instance identified in satellite altimeter data from 1993 onward) are quite different from those for longer periods in the Indo-Pacific Ocean (examples: 1960–1999 in *Alory et al*. [2007]; 1961–2008 in *Han et al*. [2010]; 1966–2007, 2000–2006, and 1993–2006 in *Nidheesh et al*. [2013]). Specifically, linear trends from relatively short records are strongly influenced by decadal variability which is not altogether well understood [*Nidheesh et al*., 2013; *Zhang and Church*, 2012]. Improved

descriptions of the temporal and spatial decadal variability will contribute to a more accurate understanding of the long-term changes of salinity, steric sea level, and ocean climate.

Earlier studies of dynamics of Indian Ocean variability motivated this study of variability of salinity anomalies. On interannual time scales, several studies document westward propagating signals in the tropical SIO and their connection with the Pacific Ocean. For instance, baroclinic waves have been reported to be transmitted within the thermocline from the western Pacific to the Indian Ocean via the Indonesian Passages [*Meyers*, 1996; *Wijffels and Meyers*, 2004; *Cai et al*., 2005; *Alory et al*., 2007]. Other studies show that El Niño Southern Oscillation (ENSO) signals are transmitted from the North Pacific Ocean to the Western Australia (WA) coast as coastally trapped waves and then radiate across the SIO as Rossby waves [*Kundu and McCreary*, 1986; *Cai et al*., 2005]. *Shi et al*. [2007] explain that little of the ENSO signal was transmitted to the Indian Ocean in the pre-1980 period, but a stronger discharge was transmitted in the post-1980 period. Their modeling work suggests that this might not be greenhouse gas induced since the multidecadal fluctuations in their results were generated by experiments in the absence of climate change forcing. Further, *Cai et al*. [2008] assess the performance of general circulation models (GCMs) from the Intergovernmental Panel on Climate Change (IPCC) Fourth Assessment Report (AR4) to transmit signals from the West Pacific to the Indian Ocean and the extent to which the thermocline shoaling in the off-equatorial SIO is attributable to this transmission. These authors find that eight models out of 22 transmit the thermocline shoaling observed from the equatorial Pacific into the off-equatorial SIO via the Indonesian Seas. This transmission occurs in those models that tend to have a greater ENSO amplitude and broader meridional extent of the ENSO anomalies.

On multidecadal timescales, several studies document contrasting mechanisms for variation of thermal structure. *Schoenefeldt and Schott* [2006] suggest that changes in the shallow meridional overturning circulation, which brings cold waters from the subtropics to the tropics, could play an important role in generating the thermocline long-term cooling trend in the subsurface tropical SIO. *Alory et al*. [2007] and *Schwarzkopf and Böning* [2011] suggest that changes in the trade-winds of the tropical Pacific Ocean, as proposed by *Timmermann et al*. [2010] and *Feng et al*. [2011], are transmitted to the tropical SIO via the Indonesian Seas and contribute to create the cooling trend. *Trenary and Han* [2008] suggest that enhanced equatorial westerly winds in the SIO, together with possible forcing from the Pacific Ocean, may contribute to the cooling as well. Other studies suggest that reductions of the Indonesian Through-Flow (ITF) transport following the 1976/1977 climate shift might also be linked to this cooling pattern and associated heave of the thermocline [*Alory et al*., 2007; *Wainwright et al*., 2008]. *Han et al*. [2010] claim that this pattern is driven by changes in the surface winds due to the increase in greenhouse gases.

Earlier studies show that remote influences from the Pacific Ocean and the modulation of the ITF (due to wind changes in the Pacific) can impact significantly on the interdecadal-to-decadal variability of the SIO [*Hirst and Godfrey*, 1993; *Reason et al*., 1996]. The Pacific Decadal Oscillation and/or the Interdecadal Pacific Oscillation (PDO/IPO)-related decadal variability of sea level in the tropical Pacific Ocean is shown to be transmitted to the SIO through the coastal waveguide and detected at the Fremantle tide-gauge in southwest WA [*Feng et al*., 2004]. Further studies show that decadal variations of the ITF and Leeuwin Current (LC) are related to Pacific Subtropical Cell (STC) variations and connected through equatorial and coastal waveguides: stronger Pacific STCs induce stronger ITF and LC [*Feng et al*., 2010]. Studies using SSH from satellite altimeters for the period 1993–2006 show a near-coherent decadal variation over most of the Indo-Pacific region characterized by a phase change at the end of the 20th century [*Lee and McPhaden*, 2008]. Those studies also reveal linkages between the Pacific and Indian Ocean STCs with a stronger Pacific STC corresponding to a weaker Indian Ocean STC, which leads to anti-correlated sea levels during the above period between the two oceanic basins [*Lee and McPhaden*, 2008].

Recent modeling studies demonstrate the importance of wind-stress forcing over the Indian Ocean in reproducing the horizontal and vertical spatial patterns observed in decadal variations of SSH, OHC and depth of the 20°C isotherm (D20) in the tropical SIO [*Nidheesh et al*., 2013; *Trenary and Han*, 2013; *Han et al*., 2014]. Specifically, *Nidheesh et al*. [2013] suggest that decadal variability in the tropical SIO is mostly influenced by regional wind stress in the SIO while the multidecadal variability (or longer term trends) is likely more influenced by the remote contribution from the Pacific Ocean via the Indonesian Seas. *Trenary and Han* [2013] also confirm that regional variability of wind-stress curl in the SIO is the main factor influencing decadal variability of dynamic variables in the tropical SIO within the 5°–17°S zonal band before 1990. They

also find that after 1990 SSH and D20 signals from the Pacific Ocean induced by decadal variability of the equatorial Pacific trade winds play a greater role in explaining the decadal variability in the tropical SIO basin. Further south (20°–30°S) local internal-ocean variability of the SIO makes an important contribution to decadal variability of SSH, sea surface temperature (SST) and D20 [*Trenary and Han*, 2013]. A detailed review of decadal and multidecadal time scale variability in dynamic variables in the Indian Ocean is provided by *Han et al*. [2014].

1.2. Contributions From Salinity to Indian Ocean Decadal Variability

In summary, most of the recent studies of decadal-scale variability and change in the tropical SIO (band around 8°S–20°S) thermocline have focused on dynamic variables and wind driven linear ocean dynamics with local and remote contributions [*Schwarzkopf and Böning*, 2011; *Nidheesh et al*., 2013; *Trenary and Han*, 2013; *Han et al*., 2014]. However, those studies have not closely considered the contributions from salinity anomalies to the decadal signature. Here we investigate the contribution of salinity anomalies at thermocline depths originating from the eastern SIO, Indonesian Seas and western tropical Pacific Ocean (WTPO) via the Indonesian Passages, to the observed decadal-to-interdecadal variability of the tropical SIO within the thermocline and primarily in the 8°S–20°S band. Specifically, we analyze the spatial patterns and decadal variability of the salinity anomaly signals that are seen to travel westward in the SIO thermocline from ocean state estimates provided by the Simple Ocean Data Assimilation version 2.2.4 (SODA).

2. Data and Methods

This study uses temperature, salinity and current speeds from the Simple Ocean Data Assimilation version 2.2.4 (SODA) [*Carton and Giese*, 2008] for the period 1950–2007 to analyze the decadal variability in the Indo-Pacific Ocean. These data have been recently evaluated for their potential to understand decadal ocean and climate variability of the Indo-Pacific Ocean—specifically it was demonstrated that these data are potentially useful for decadal variability studies of steric sea level [*Vargas-Hernandez et al*., 2014]. Those variables were annually averaged since the interest here is on the decadal time scales. In most of the analysis (unless otherwise stated) a 10 year low-pass Butterworth filter (LP10 hereafter) was applied to remove the higher frequency variations shorter than 10 years, thus retaining only the low-frequency (periods $\geq$ 10 years) variability in the data.

First, the long-term linear trends in steric SSH and halosteric SSH (HlSSH) were estimated. The SSH was calculated in terms of the dynamic height anomaly across the 5–729 m depth range and dividing it by the gravitational acceleration. The dynamic height anomaly was calculated using the TEOS-10 and Gibbs Seawater Oceanographic Toolboxes available from http://www.teos-10.org/. The ThSSH was calculated in the same manner as the steric SSH but imposing a constant salinity value of 34 g kg^{-1} to only capture the SSH changes due to thermal expansion of the water column. The HlSSH was estimated by subtracting the ThSSH from the steric SSH.

Salinity anomalies at different isotherm depths were calculated by first linearly interpolating the vertical temperature structure to the selected isotherms—to spatially characterize depth variations in the thermocline shape—and then similarly estimating the corresponding salinity values along this thermocline surface. This study primarily examines salinity anomalies on the D20 in order to estimate salinity changes (in space and time) that are separated from the dynamic heave of the thermocline. Linear long-term trends in steric SSH, ThSSH, vertically integrated salinity and D20 anomalies were calculated by finding the linear coefficients that best fit the data in a least-squares sense for the period 1950–2007.

A two-dimensional form of radon transform (2D-RT) analysis [*Challenor et al*., 2001] was used to estimate the speeds of the westward moving signals across meridionally averaged zonal bands in the tropical SIO, western tropical North Pacific Ocean (NPO) and South Pacific Ocean (SPO). These data were gap-filled using Gaussian interpolation, for example, in the case of very small islands and westward filtered to only retain westward traveling signatures in the data prior to performing the 2D-RT analysis. Specific details of the RT and 2D-RT methods used here and some applications are provided by *Challenor et al*. [2001] and *Maharaj et al*. [2009].

A lagged linear regression (LLR) analysis was used to identify and better understand relationships with the dynamic forcing and regions that contribute to, and underpin, the spatial patterns of the salinity anomalies

on a specific isotherm used to characterize the thermocline surface. This technique is useful in this study to identify the different sources of salinity anomalies. Each spatial point time series of salinity anomalies is regressed onto a selected time series at key locations, such that

$$S'(t)=a[S'(t+L_i)]+b, \tag{1}$$

where the LP10 salinity anomaly S', at time t, is expressed as the salinity anomaly S' time series at lag L_i (source at key location), with regression coefficient a and residual b. All possible lags within $\pm$10 years with a time step of 1 year were searched to find the combination that corresponds to the maximum correlation coefficient squared ($R^2 \geq 0.3$ and significant at $\geq$95% level) associated with the maximum variance accounted for between the linear model fitted S' time series at each grid point and the S' time series at key locations.

A standard empirical orthogonal function (EOF) analysis was also applied to identify the main decadal coherent patterns in the data, and to quantify the corresponding variance explained in the important EOFs, and to estimate the possible contributions from local (eastern SIO) and remote (WTPO) sources. Using the covariance matrix in the EOF analyses, the units of the fields are formally carried by the principal component (PC) time series, while the EOF spatial patterns are dimensionless [e.g., *Venegas*, 2001]. Here however, the PCs are also dimensionless since the eigenvectors derived from the EOF analysis were scaled so that the norm of each is 1. Hence, the PC time series are readily plotted together with the IPO index for visual comparison.

Finally, vertical profiles from the 2009 version of the CSIRO Atlas of Regional Seas (CARS) [*Ridgway et al.*, 2002] were used here to calculate the speeds of the first four baroclinic modes. The baroclinic speeds must be calculated for the whole water column (from surface to ocean bottom) as the boundary conditions for the Sturm-Liouville differential equations (see Equations (2) and (3)) assume that the speeds are zero at the ocean bottom. Although SODA provides vertical profiles down to 5374 m depth, the SODA data used in the present study comprise only depths down to 2125 m as we are more confident of SODA in the shallower depths where more historical observations have contributed to this reanalysis product. Instead, as a seasonal (monthly averaged) climatological product, CARS was used because it provides vertical profiles up to 5500 m depth for the locations of interest. To calculate the baroclinic wave speeds, c_m, the following system of equations, in terms of vertical structure functions ($\hat{h}_m(z)$ and $\hat{p}_m(z)$), were solved (see pages 159–162 from *Gill* [1982] for more detail):

$$\frac{d^2\hat{h}_m}{dz^2}+\frac{N^2}{c_m^2}\hat{h}_m=0 \tag{2}$$

$$\frac{d}{dz}\left(\frac{1}{N^2}\frac{d\hat{p}_m}{dz}\right)+\frac{1}{c_m^2}\hat{p}_m=0, \tag{3}$$

where $N^2(z)$ is the buoyancy frequency as a function of depth given by

$$N^2=-\frac{g}{\rho}\frac{d\rho}{dz} \tag{4}$$

Here $g = 9.8$ m s^{-2} is the gravitational acceleration and $\rho=\rho(z)$ is the vertical density profile. N^2 and ρ were calculated from the time-averaged temperature and salinity at two locations in the western tropical NPO (12.25° N, 159.25° E) and in the SIO (12.25° S, 90.25° E) using the Gibbs SeaWater (GSW) Oceanographic Toolbox (http://www.teos-10.org). The eigenvalue and eigenvector problem was solved using a script written by J. Klinck and available at the Woods Hole SEA-MAT site (http://woodshole.er.usgs.gov/operations/sea-mat/).

3. Results

3.1. The Dominant 58 Year Trend Mode

A signal in the 10°S–20°S zonal band that connects the WTPO with the tropical SIO was identified in the multidecadal trend of steric, thermosteric and halosteric sea surface heights (SSH, ThSSH and HlSSH respectively, Figures 1–1c). The thermosteric anomaly in this band (Figure 1b) shows a lowering of sea level across the Indian Ocean connected to the Pacific Ocean through the Indonesian Seas. The increase in salinity in the band (Figures 1d) is associated with a halosteric reduction (Figure 1c) in the contribution to SSH (Figure 1a) that acts in unison with the thermosteric reduction (Figure 1b), although it is interesting to see

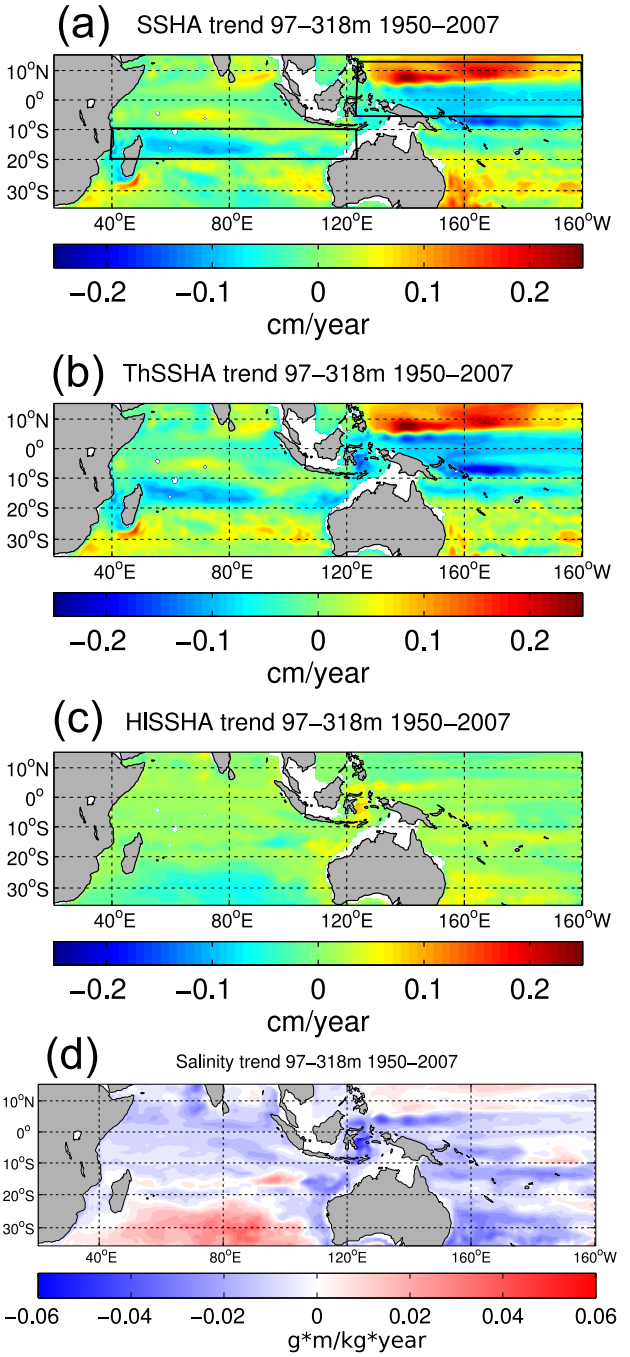

Figure 1. Linear trends from 1950 to 2007 of (a) steric sea surface height anomalies (SSHA), (b) thermosteric sea surface height anomalies (ThSSHA), (c) halosteric sea surface height anomalies (HISSHA), and (d) vertically integrated salinity over the upper 97–318 m. The signal of interest in the linear trend along the tropical SIO is depicted with a black box in Figure 1a.

that the ThSSH shows a weakened lowering from about 90°E to 110°E (Figure 1b). It is also interesting to see that the decrease in salinity in the Banda Sea (Figures 1d and 2) which causes positive HISSHA (Figure 1c), due to the strong freshening, tends to partially offset the effect of the negative trend in SSH due to the change in temperature in that region.

An EOF analysis applied to the depth of the thermocline in this region showed that the dominant mode was the multidecadal trend linked to the Pacific Ocean. The first EOF of anomalies in the depths of the 14°C and 20°C isotherms (D14 and D20 anomalies respectively) also capture the link in the linear trend between the two ocean basins (not shown here). This multidecadal linear trend has been documented previously [*Alory et al.*, 2007; *Timmermann et al.*, 2010; *Schwarzkopf and Böning*, 2011; *Nidheesh et al.*, 2013; *Trenary and Han*, 2013], except to note that SODA 2.2.4 reproduces it. Instead, the main focus here is the decadal variability pattern observed in the salinity anomalies on the D20 surface as a function of time.

3.2. EOF Analysis of Salinity Anomalies on D20

In order to identify the main decadal patterns and quantify the possible contributions from the different regions, an EOF analysis of the salinity anomalies on D20 was applied. For the purposes of this study, the EOF analysis has the advantage of decomposing the large three-dimensional field (salinity anomalies in horizontal space and time) into only a few modes of variability that describe a high percentage of the overall variance in the data, with the lowest order modes likely to be physically meaningful. The EOF analysis of the nondetrended LP10 salinity anomalies on D20 shows that EOF1, EOF2 and EOF3 are independent modes, based on evaluation of the errors in the eigenvalue spectrum according to *North et al.* [1982], and explain 39%, 18% and 12% of the total variance respectively (Figures 3a–3f).

EOF1 shows a strong pattern that extends from the eastern SIO (20°S–25°S, around 100°E) to the western tropical SIO (10°S–20°S), explaining most of the variance in the region (Figures 3a and 3b). It

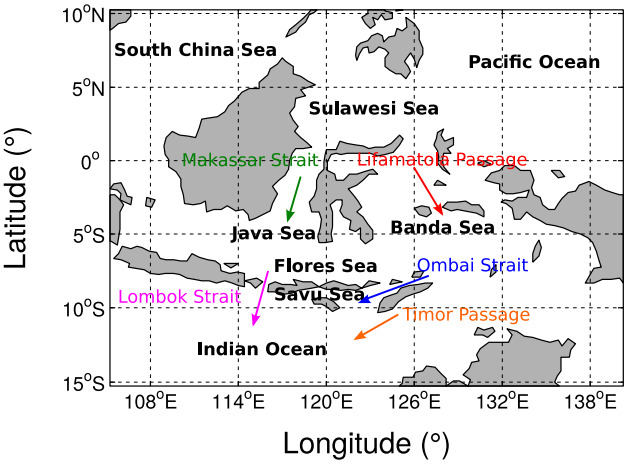

Figure 2. Key flow passages and straits in the Indonesian Seas.

shows a salinity anomaly around the edge of the subtropical gyre that became less saline from 1980 until the late 1990s, then rapidly increased in salinity.

EOF2 is associated with the multidecadal trend (Figures 3c and 3d) as it disappears when an EOF analysis is applied to the detrended data (not shown here). It is also consistent with the main signal in the spatial pattern of the salinity trend discussed in section 1.2 (Figure 11d). Unlike other variables that contribute to dynamic height changes (for instance OHCA, SSH, D20), the multidecadal trend is not the dominant mode for salinity anomalies on D20. As already mentioned, we focus our attention on the decadal-to-interdecadal signals. Thus, we hereafter detrend the LP10 SODA data to remove the multidecadal linear trend signal.

EOF3 appears to be the salinity response to decadal-to-interdecadal ocean climate variability associated with the IPO, as the EOF3 time series (otherwise known as PC3) is significantly correlated with the IPO index (Figure 3f). The EOF3 spatial pattern provides evidence for a connection between the Indonesian Seas and the tropical western NPO and SPO; however the pattern does not penetrate into the tropical SIO beyond about 110°E (Figures 3e and 3f). Signals in SSHA related to large-scale IPO changes have been reported to connect the western tropical Pacific Ocean with the Indian Ocean [*Vargas-Hernandez et al*., 2014]. Hence, the signal in salinity anomalies at D20 observed in EOF3 (Figures 3e and 3f) is likely to be part of this same signal in SSHA, both related to IPO changes.

Finally, EOF4 and EOF5 (Figures 3g–3j) account for 6% and 5% of the total variance respectively and are coupled modes according to the *North et al*. [1982] criterion for mode independence. Together, these modes highlight the important relationship between the variability in the WTPO and tropical SIO. EOF4 highlights the connection between the variability in the western tropical SPO with that in the Indonesian Seas and tropical SIO, and extending to the western tropical SIO near Madagascar (Figures 3g and 3h). EOF5 shows a continuous salinity pattern that starts in the western tropical NPO and extends through the Makassar and Lombok Straits and leaks into the tropical SIO at around 10°S, 100°E, continuing to the central tropical SIO (Figure 3i). This pattern appears to be associated with the salinity anomaly contribution from the western tropical NPO into the tropical SIO. Furthermore, it appears to be that EOFs 4 and 5 are also capturing details of the evolution of the salinity anomaly in the band (10°S–20°S) and in the longitudes 70°E–100°E, that is the place when EOF1 shows the strongest signal.

3.3. Slow Westward Moving Signals on Decadal Time Scales

We examined westward traveling salinity signals along two zonal bands that appear to be connected, one meridionally averaged from 6.25°S to 12.25°N in the WTPO and another one meridionally averaged from 9.25°S to 19.25°S in the tropical SIO (see boxes in Figure 1a). Here we can see the transmission of westward moving features on interannual and decadal time scales via the Indonesian Seas (Figure 4). The westward moving signals of annual D20 and OHC anomalies (Figures 4a and 4c) appear to travel from 159.25°E to 40.25°E in about 4 years, consistent with linear Rossby wave propagation as reported in the literature [*Schwarzkopf and Böning*, 2011], where first baroclinic Rossby wave speeds are calculated as $C_R = \beta(c_1^2/f^2)$ (c_1 is the first baroclinic mode gravity wave speed [*Chelton et al*., 1998], f is the Coriolis parameter and β is the meridional variation of the Coriolis parameter), and can be confirmed using radon transform analysis, or similar, to estimate the speeds from Hovmöller plots. In contrast to the westward movement of D20 and OHC anomalies, annual salinity anomalies on the D20 surface travel much more slowly, taking longer than 10 years to traverse the same zonal distance, although with more discontinuity in its pathway between

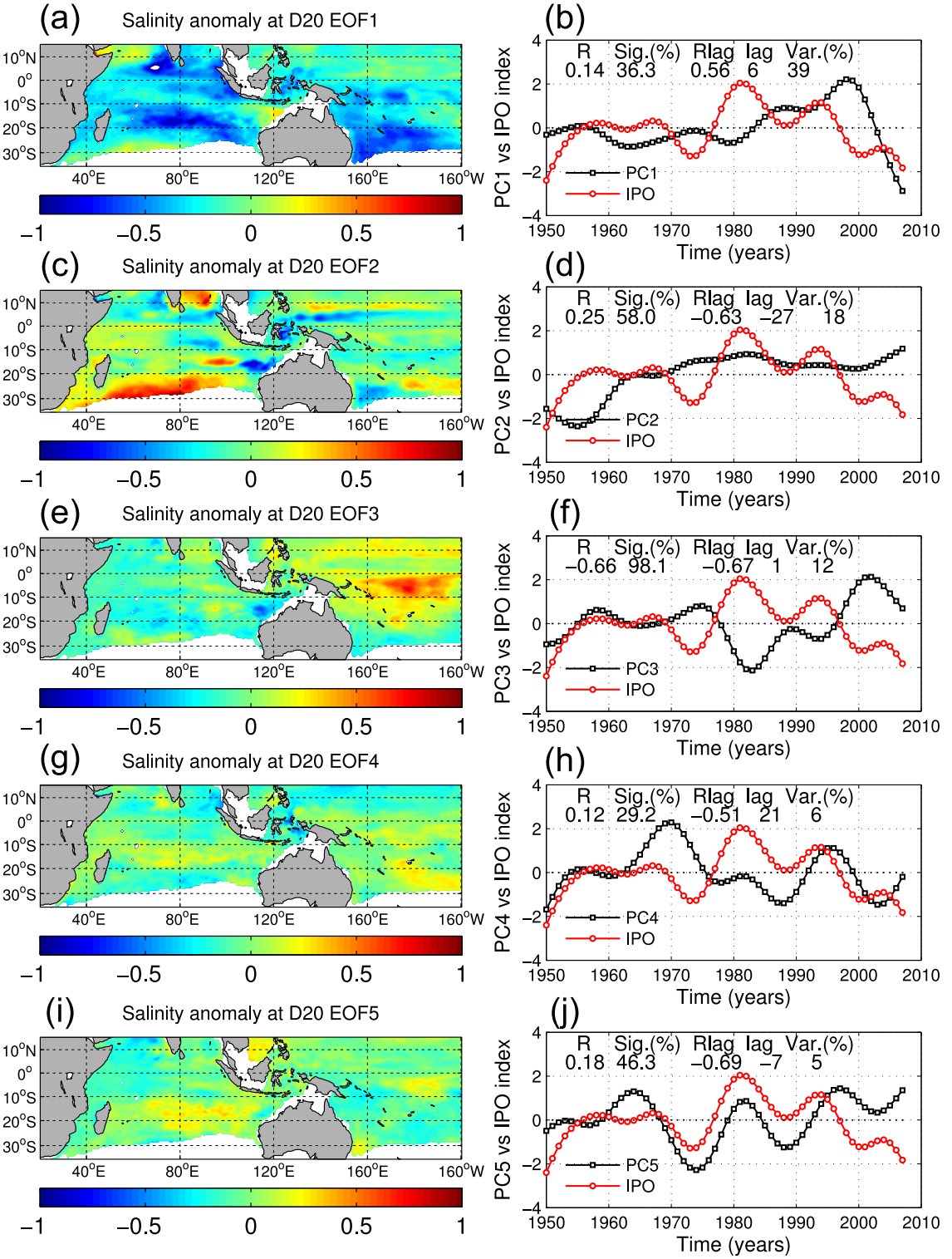

Figure 3. Five leading modes from the EOF analysis on the LP10 salinity anomalies on D20. Panels on the left show the EOF mode spatial loading and panels on the right show the corresponding principal components (PCs, time series) of the EOFs. The PCs were compared with the LP10 IPO index. The correlation coefficient (R), significance (Sig.), cross correlation coefficient (Rlag), lag in years (lag) of the PCs with the IPO index and the variance (Var.) explained by each mode are shown. Units are nondimensional. The magnitude of the detected signals ranges from −0.25 to 0.25 g/kg.

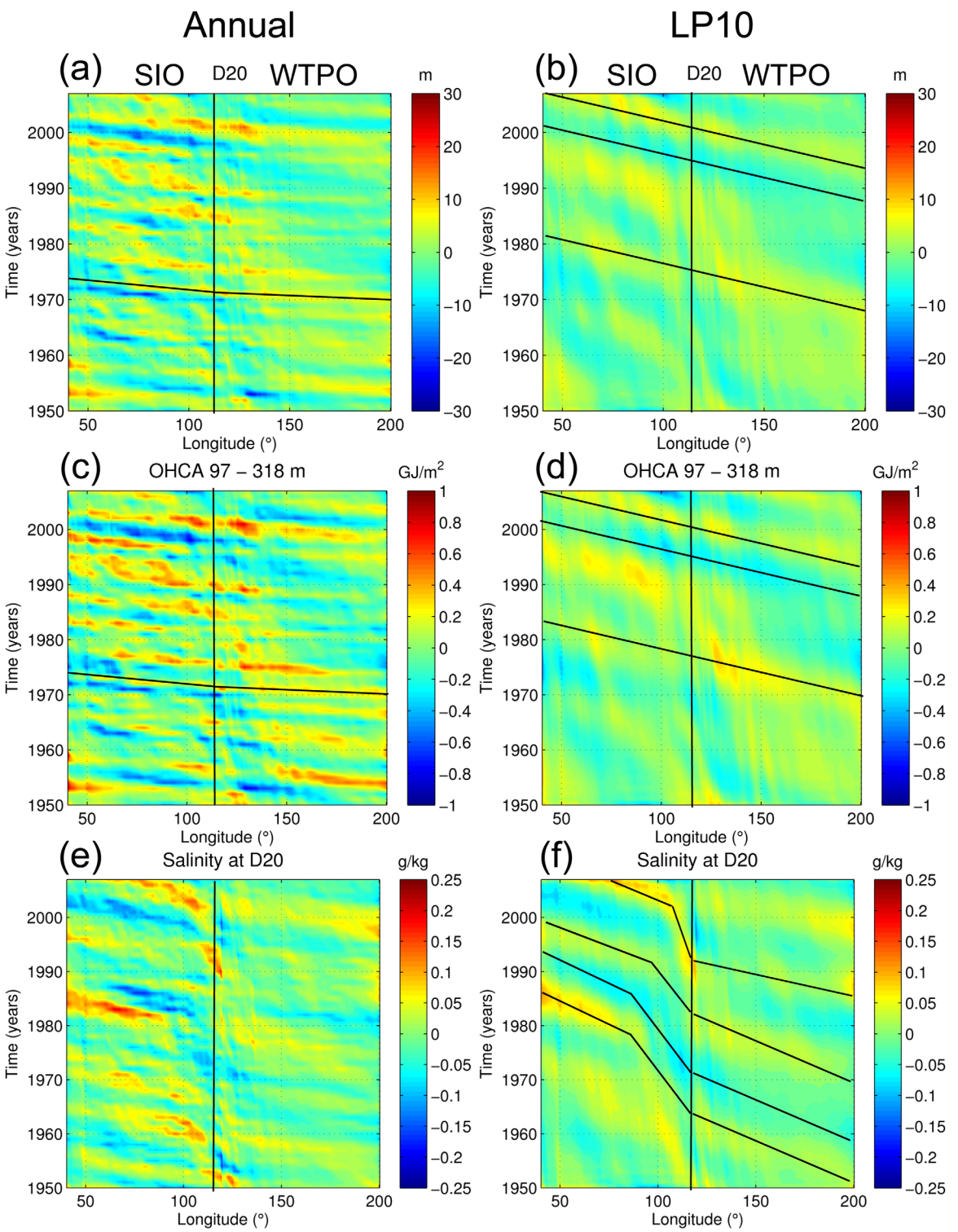

Figure 4. Hovmöller plots of (a, b) D20 anomalies, (c, d) OHCA calculated from 97 to 318 m and (e, f) salinity anomalies on the D20 surface for the meridionally averaged bands corresponding to 9.25°S–19.25°S across the tropical South Indian Ocean, and 6.25°S–12.25°N across the western tropical Pacific Ocean. (left) Detrended annual Hovmöller plots and (right) detrended 10 year low-pass Butterworth-filtered Hovmöller plots. Oblique lines in Figures 4a and 4c correspond to the first baroclinic Rossby wave propagation speed and on the right plots indicate the slow westward traveling signals.

WTPO and SIO (Figure 4e). After applying the LP10 filter to the data we observed this slow westward movement in the three variables, but more clearly in the salinity anomalies, taking around 10 to 20 years to travel along the Indo-Pacific transect (Figures 4b, 4d, and 4f). Interestingly, these salinity anomalies traveled much

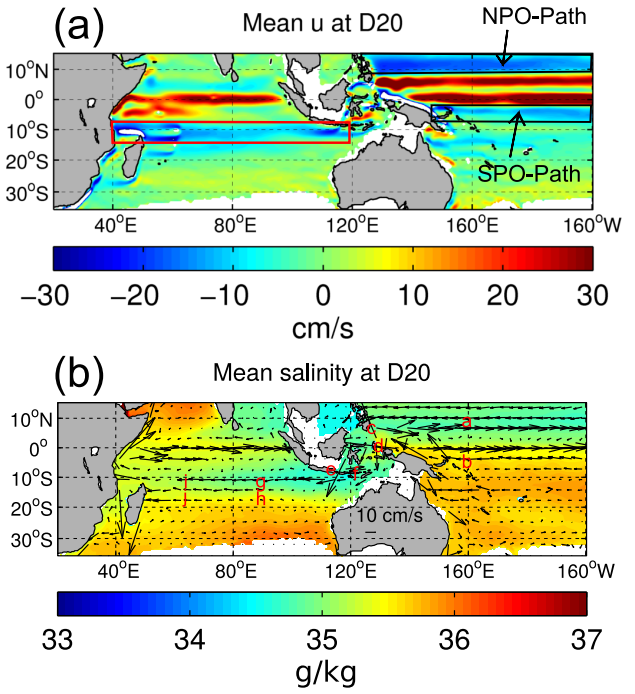

Figure 5. (a) Mean zonal velocities in cm s^{-1} (negative values indicate westward direction and positive values indicate eastward direction) on D20, and (b) annual mean salinity field and velocity vectors on D20. Boxes in Figure 5a indicate the ocean pathways and red letters in Figure 5b indicate the chosen locations along the NPO, SPO and SIO pathways to study decadal-scale transmission signals from the WTPO into the SIO.

slower than the D20 and OHC anomalies in the SIO, specially in the eastern tropical SIO (90°E–119°E). Hence, we identified signals of salinity anomalies on decadal and multidecadal time scales (Figure 4f). The following questions arise from Figure 4: What mechanism explains this slow westward signal in the salinity anomalies on D20? Could it be salinity advection associated with the mean flow or perhaps nonlinear Rossby wave propagation and/or the effects of higher order baroclinic Rossby wave modes interacting with the mean flow? What are the possible sources from the Indian Ocean and Pacific Ocean to the time scales observed in the data and the connections implied?

3.4. Ocean Pathways

To consider salinity advection as a hypothesis, the annual mean zonal flow at different isotherm depths was explored (not shown here). We found that at the depth of 20°C isotherm (D20), the westward flowing North and South Equatorial Currents in the Pacific may supply water to the SIO by two pathways. One pathway comes from the western tropical NPO (NPO-path, Figure 5a) around 9°N–12°N which goes all the way down through the Makassar Strait to the Banda Sea and exits the Indonesian Seas through Lombok Strait, and then further east through Ombai Strait (in Savu Sea) and Timor passage [*Wijffels et al*., 2008, Figures 1 and 2]; the other pathway comes from the western tropical SPO (SPO-path, Figure 5a) passing along the coast of Papua New Guinea, continuing through Lifamatola Passage to the Banda Sea, and leaving the interior seas through Ombai Strait and Timor Passage (Figure 2). Both flows along the NPO-path and SPO-path seem to merge together in the eastern tropical SIO around 12°S in the South Equatorial Current.

The annual mean salinity on D20 provides an impression of how low salinity water from the WTPO penetrates into the Indonesian Seas and then the SIO following the NPO-path and SPO-path (Figure 5b). The NPO flow path carries low salinity waters ($<$ 35) while the SPO flow path carries saltier waters ($>$35.5). Strong freshening in the Indonesian Seas, due to high precipitation rates in that region, contribute to the fresher waters advected into the tropical SIO (Figure 5b). It is also noticed that the eastern Banda Sea is saltier than the western Banda Sea and Flores Sea.

3.5. Vertical Structure of the Salinity Anomalies Along the Oceanic Pathways

Here we show that decadal variability of salinity anomalies may not be influenced by the vertical heave of the thermocline caused by waves propagation. Salinity changes on isotherms are largely unaffected by the heave due to vertical excursions of the thermocline that characterize wave propagation (in particular, Rossby wave propagation), and thus are most likely to be caused by other processes (Figure 6). A caveat here is that the meridional thermocline excursions due to Rossby wave propagation play a role in these associated salinity anomalies. Salinity anomalies along the NPO-path (locations a, c, and e in Figure 5b) show decadal variability corresponding to warmer isotherms ($\geq$20°C) in shallower depths at locations in the NPO and at the mouth of Lombok Passage (Figures 6a, 6c, and 6e, respectively). Salinity anomalies along the SPO-path show strong decadal-to-interdecadal variability (locations b and d in Figure 5b) on colder isotherms that reached the 16°C isotherm at location b and d (Figures 6b and 6d, respectively) and down to

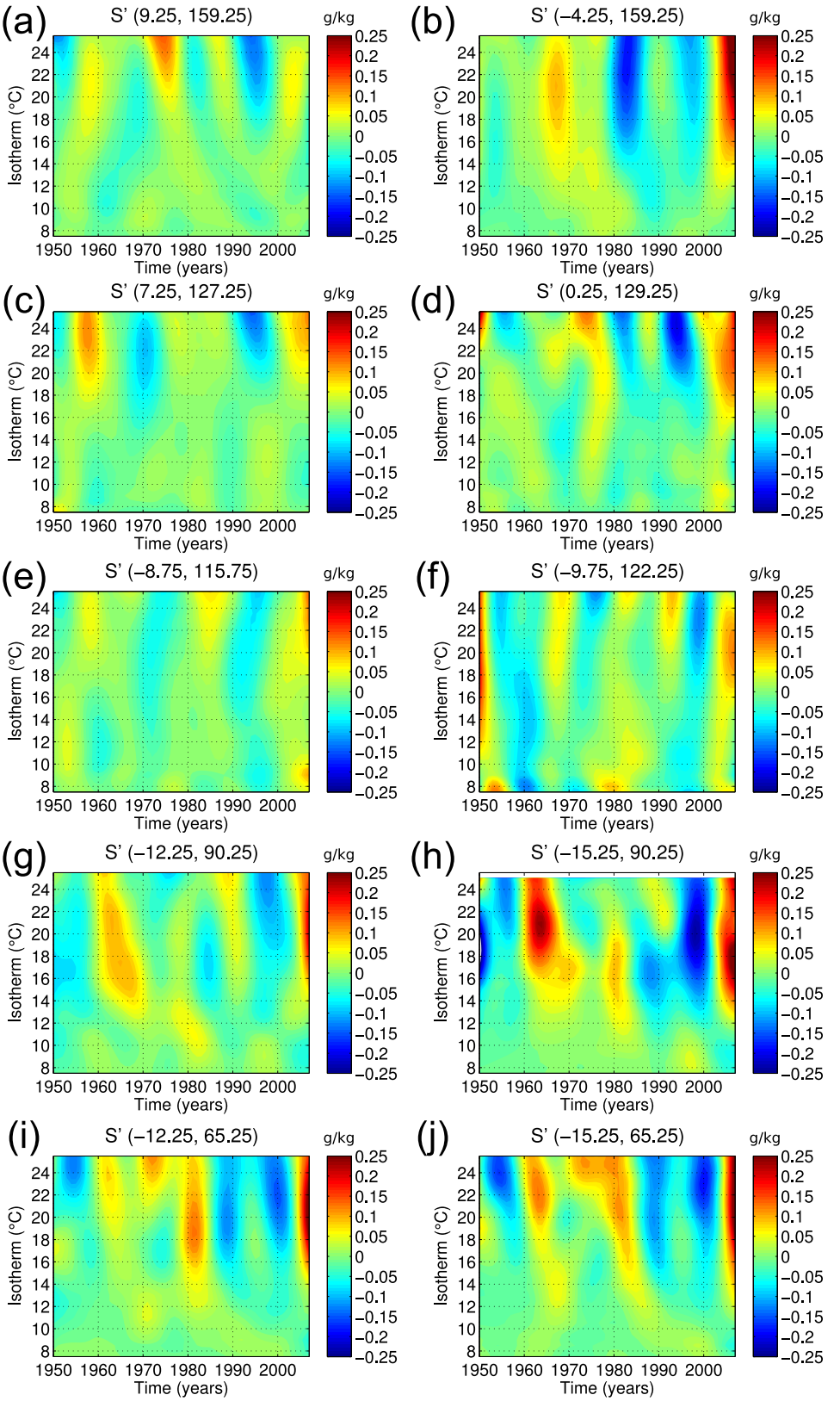

Figure 6. Absolute salinity anomalies (*S'*) at several isotherms over time at 10 locations given as in Figure 5. The location in coordinates (latitude, longitude) are shown on top each map. Detrended and LP10 data were used in all plots.

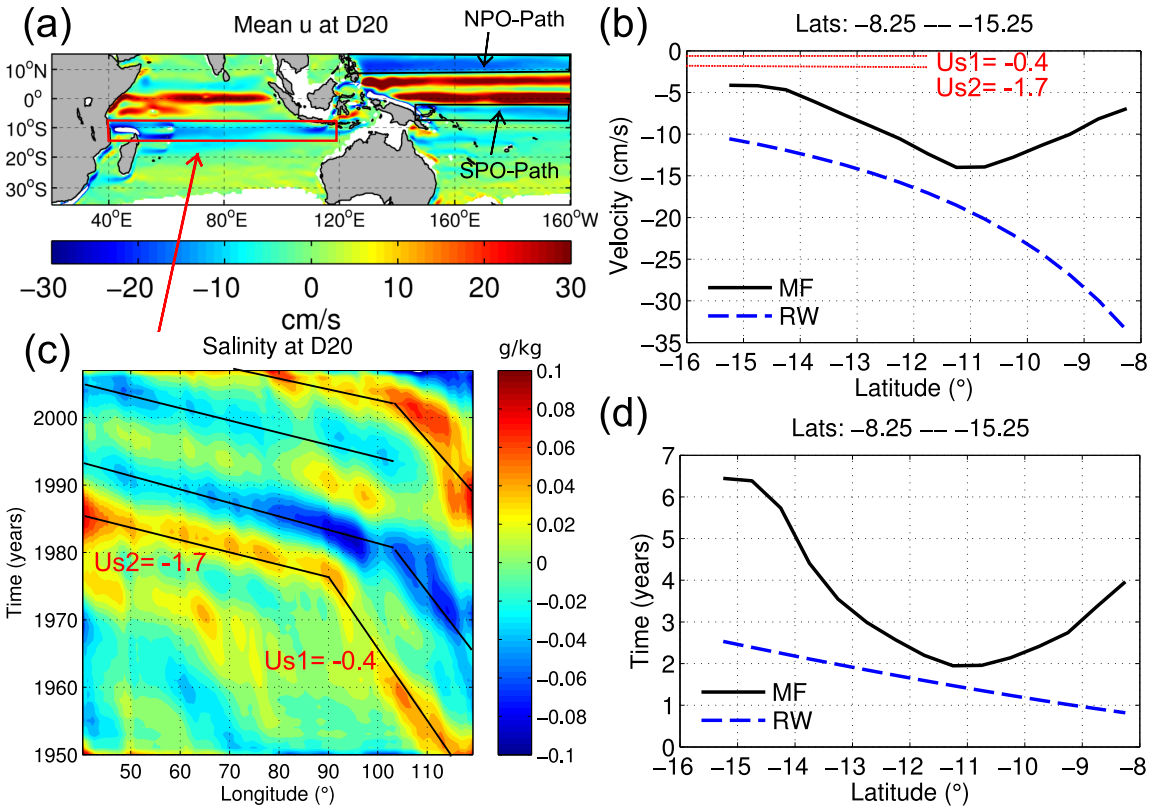

Figure 7. (a) Mean zonal velocities in cm s^{-1} (negative values indicate westward direction and positive values indicate eastward direction) on D20; (b) mean zonally averaged (40.25°E–119.25°E) speeds (cm s^{-1}) as a function of latitude on D20 from SODA (mean flow MF, black bold line) and the first baroclinic-mode Rossby wave (RW) speed estimates from theory (blue dashed line), $C_R = \beta(c_1^2/f^2)$, where c_1 is the theoretical gravity wave speed from *Chelton et al.* [1998], f is the Coriolis parameter and β is the meridional variation of the Coriolis parameter; (c) Time-longitude (Hovmöller) plot of meridionally averaged (8.25°S–15.25°S) and detrended LP10 salnity anomalies (g kg^{-1}) on D20 across the tropical Indian Ocean; and (d) Mean transit times for zonal "flow"(or propagation) u, and C_R to cross the Indian Ocean (40.25°E–119.25°E) as a function of latitude. The signal speeds (Us1 and Us2) from the 2D-RT are also provided in red.

the 10°C isotherm at the location f in the Ombai Strait (Figure 6f). However, salinity anomalies in the Ombai Strait (location f) region are difficult to interpret as the region also connects with flows from Makassar Strait [*Wijffels et al*., 2008], where this location might be influenced by flows coming from both the NPO and SPO. Once the flows have merged in the SIO, the salinity anomalies showed similar decadal variability, but more intensely in higher latitudes (locations g, h, i and j in Figure 5b and Figures 6g–6j).

3.6. Speeds of Westward Moving Salinity Anomalies Across the Tropical South Indian Ocean

To understand the possible mechanism associated with the westward moving salinity anomalies in the SIO we have mapped the mean zonal flow at D20 (Figure 7a) and also compared the speeds of the westward moving salinity anomalies with: (a) the mean zonally averaged (40.25°E–119.25°E) speeds of the flow and (b) the first baroclinic-mode Rossby wave speed estimates from theory (Figure 7b) as a function of latitude on D20. We discuss these comparisons in the next sections. Moreover, a 2D-RT analysis applied to salinity anomalies on D20 in the tropical SIO shows that the westward (indicated by the negative sign in all panels in Figure 7) speeds of the anomalies were slower in the eastern tropical SIO between 90°E and 119°E (speed around 0.4 cm s^{-1}) than in the western tropical SIO between 40°E and 90°E (speed around 1.7 cm s^{-1}) (Figure 7c). Before the mid-1970s the anomalies take around 22–25 years to travel from 119°E to 90°E and around 10 years to travel from 90°E to 40°E. After the mid-1970s the anomalies with speeds of 0.4 cm s^{-1} appear to travel shorter distances from 119°E to 105°E (Figure 7c).

3.7. Rossby Wave and Salinity Anomaly Speeds

Are the speeds of the observed decadal signals comparable to linear first baroclinic mode Rossby waves? To answer this question theoretical long (first baroclinic mode) Rossby wave speeds were compared to the salinity anomaly speeds from the LP10 Hovmöller plots. Rossby wave speeds range between 33 and

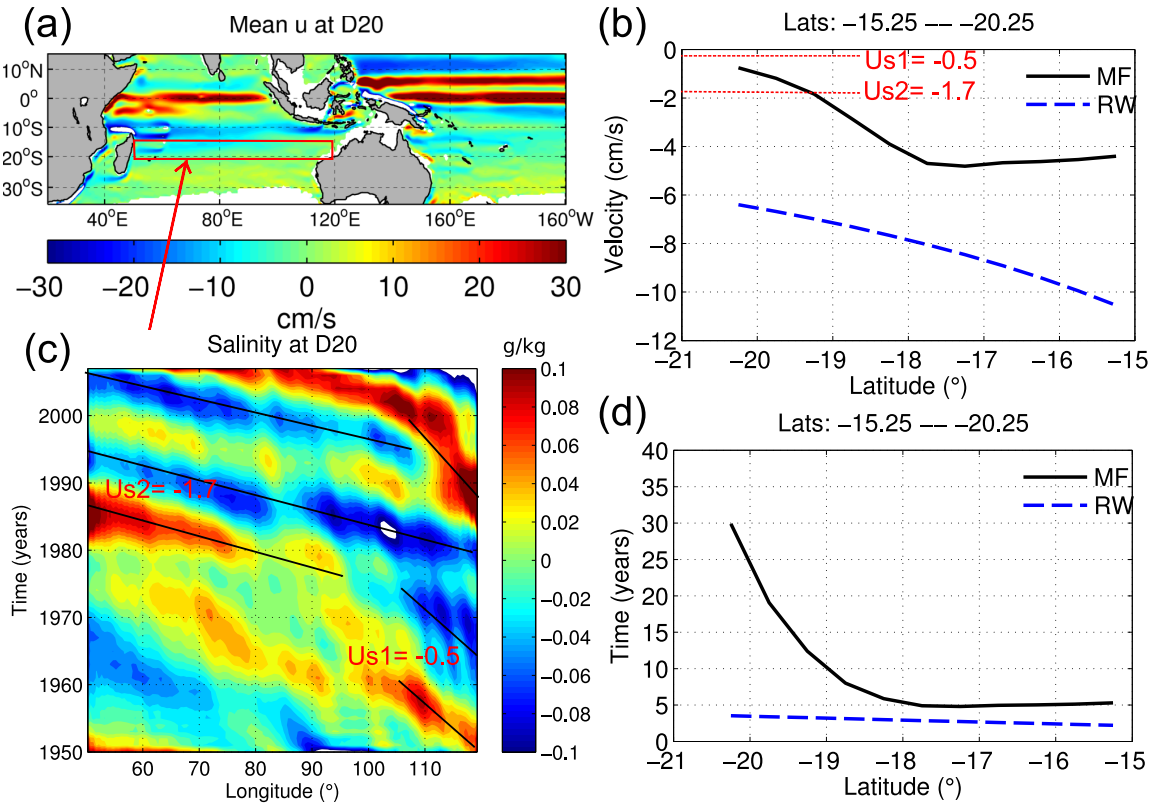

Figure 8. As Figure 7 but for: 15.25°S–20.25°S and 50.25°E–119.25°E.

10 cm s^{-1} from 8.25°S to 15.25°S respectively, and are thus at least one order of magnitude larger than the estimated speeds of the salinity anomalies in the SODA data (Figures 7b and 7c). Rossby waves take a maximum time of 2.5 years to cross the tropical SIO whereas the transit time of the salinity anomalies is around 16 years at the average latitude of 11.75°S and at a constant westward speed of 1.7 cm s^{-1} (Figure 7d). Hence, linear Rossby waves can not really be the responsible mechanism governing the slow speeds of these salinity anomalies in the low latitudes.

3.8. Mean Flow and Salinity Anomaly Speeds

Are perhaps the speeds of the salinity anomalies on D20 comparable to the zonal mean flow in the tropical SIO? The zonally averaged flow shows a minimum speed of about 4.5 cm s^{-1} around 15°S and a maximum speed of 14 cm s^{-1} around 11°S which are both also larger than these characteristic salinity anomaly speeds (Figure 7b). The mean flow takes between 2 and 6.5 years to traverse the tropical SIO depending on the latitude (Figure 7d). Although the westward speeds of the mean flow are still larger than the subject salinity anomalies, the pathway is nevertheless consistent. Therefore, we also explored other meridionally averaged bands in the tropical SIO to understand the possible influence from the Indonesian Sea waters.

Meridionally averaged westward salinity anomalies further south (15.25°S–20.25°S) across a region with slower zonal mean flow (although still influenced by waters from the Indonesian Seas, Figure 8) show similar speeds as those from the analysis between 8.25°S and 15.25°S. However, the salinity anomaly signals with speeds around 0.5 cm s^{-1} in the eastern SIO have a reduced westward penetration, and the decadal signals with westward speeds of 1.7 cm s^{-1} become stronger.

Still further south, between 20.25°S and 25.25°S where there seems to be no influence from waters from the Indonesian Seas, the slowest salinity anomaly signal in the eastern SIO disappears from the mid-1970s onward, but is evident prior to the mid-1970s (Figure 9). This latter band is more dominated by decadal signals with westward speeds around 1.7 cm s^{-1} that may be locally generated in the SIO. The zonal flow along this band is eastward between 22.5°S and 25.25°S and westward between 20.25°S and 22.5°S, whereby the westward speed is comparable to the slowest westward traveling salinity anomalies. The presence of

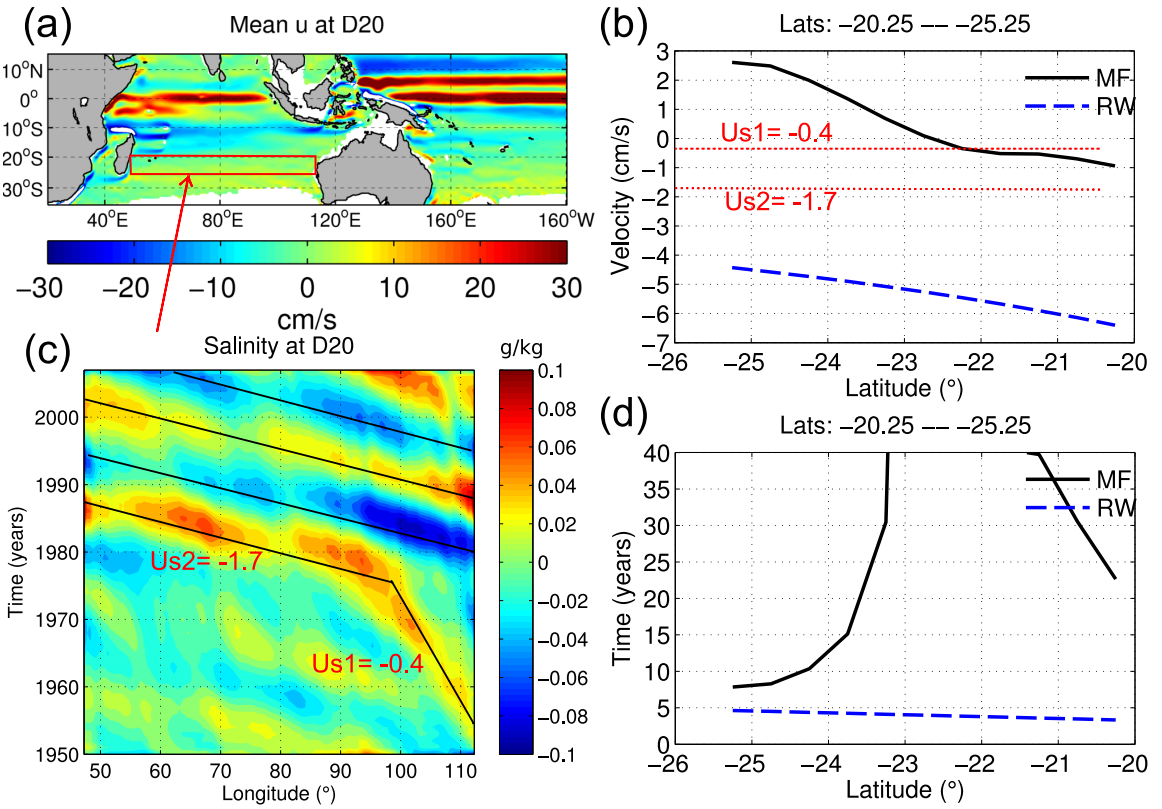

Figure 9. As Figure 7 but for: 20.25°S–25.25°S and 47.25°E–112.25°E.

westward-traveling salinity anomalies on decadal times scales along the 20.25°S–25.25°S band suggest that the mean flow might not be the only mechanism governing the westward movement of those signals.

Similar analysis was applied to the flows along the NPO-path and SPO-path in the WTPO to explore the possibility that the salinity anomaly signals in the tropical SIO (8.25°S–15.25°S) at least partly originated in the WTPO (not shown here). The strongest signal along the NPO-paths shows a speed of around 1.3 cm s^{-1} which is comparable to the decadal salinity anomaly speeds identified in the tropical SIO. The speeds of these salinity anomalies are also comparable to the zonal flow around 8.25°N but in general the flow is faster for higher latitudes. The transit time of the signal across 127.25°E–160.25°W is around 19.4 years. The strongest signal along the SPO-path travels slowly with westward speeds of around 0.8 cm s^{-1}. This is close to the mean flow speeds at 6.25°S and 9.25°S but slower than the mean flow speeds at other latitudes. The westward transit times from 119.25°E to 160.25°W are about 35 years for the salinity anomalies and 20 years for the slowest flow speed.

3.9. Higher Order Baroclinic-Mode Rossby Waves

We have established that the identified westward speeds of salinity anomalies are too slow to be explained by the westward propagation of linear first baroclinic-mode Rossby waves or by the mean westward flow speeds. To extend our analysis, we consider a baroclinic mode analysis, using the buoyancy frequency (N^2) from the time-averaged temperature and salinity profiles using the CARS data (www.cmar.csiro.au/cars), at two key locations (12.25°S, 90.25°E and 15.25°S, 90.25°E) within a zonal band in the tropical SIO where the local mean flow meet the oceanic waters from the Indonesian Seas (inside red box in Figure 7a). This analysis was undertaken to assess whether higher baroclinic modes might help to explain the slow salinity anomaly speeds identified in the SIO. Our analysis shows that the fourth (at 12.25°S, 90.25°E) and third (at 15.25°S, 90.25°E) baroclinic-mode Rossby wave speeds (1.7 cm s^{-1}) match the salinity anomaly signal speeds in SODA (Figures 10a and 10b, respectively).

Further, the horizontal velocity function ($\hat{p}_m(z)$) (for more details, see *Gill* [1982, pp. 159–162]) of the fourth baroclinic mode (m4) at 12.25°S, 90.25°E is characterized by the zero-crossing corresponding to the

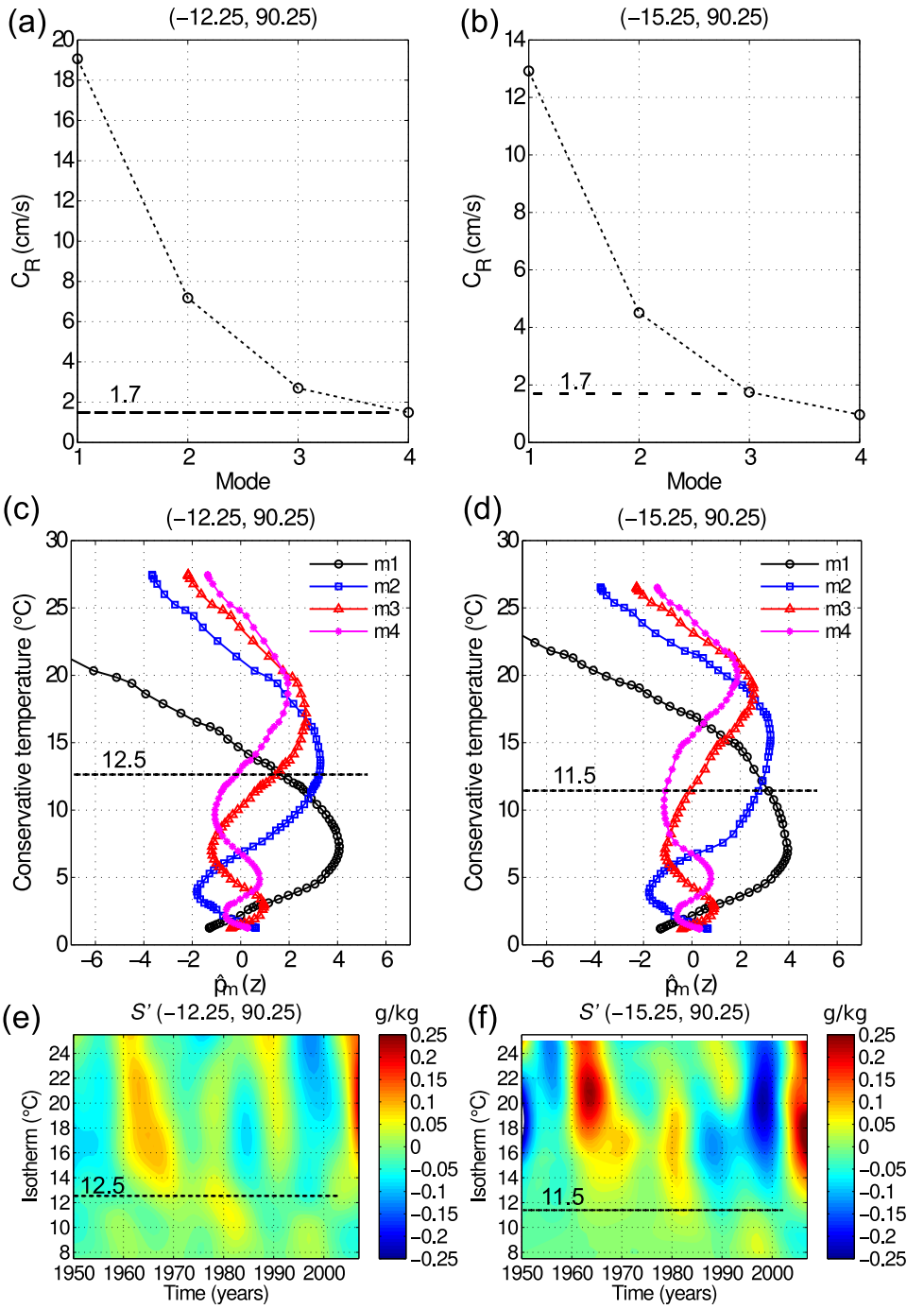

Figure 10. First four baroclinic modes (m1, m2, m3 and m4) at (a, c) 12.25°S, 90.25°E and (b, d) 15.25°S, 90.25°E in the tropical SIO and (e, f) their associated absolute salinity anomalies (S') at several isotherms over time, respectively; (a, b) Rossby waves speeds given by $C_R = \beta(c_m^2/f^2)$, where c_m is the gravity wave speed with values of $c_1 = 2.8$ m s^{-1}, $c_2 = 1.7$ m s^{-1}, $c_3 = 1.1$ m s^{-1} and $c_4 = 0.8$ m s^{-1}; (c, d) Horizontal velocity (or pressure perturbation) eigenfunctions $\hat{p}_m(z)$. The most recent version of CARS (www.cmar.csiro.au/cars) data set was used.

conservative temperature, and hence depth of, 12.5°C (Figure 10c) which corresponds well with the vertical scale of the salinity anomalies from the surface to this isotherm (Figure 10e). Similarly, the third baroclinic mode (m3) at 15.25°S, 90.25°E is characterized by the zero-crossing at the conservative temperature (depth) of 11.5°C (Figure 10d) which also corresponds well with the vertical scale of the salinity anomalies at this location (Figure 10f). It would be interesting to know whether and how these higher order baroclinic-mode

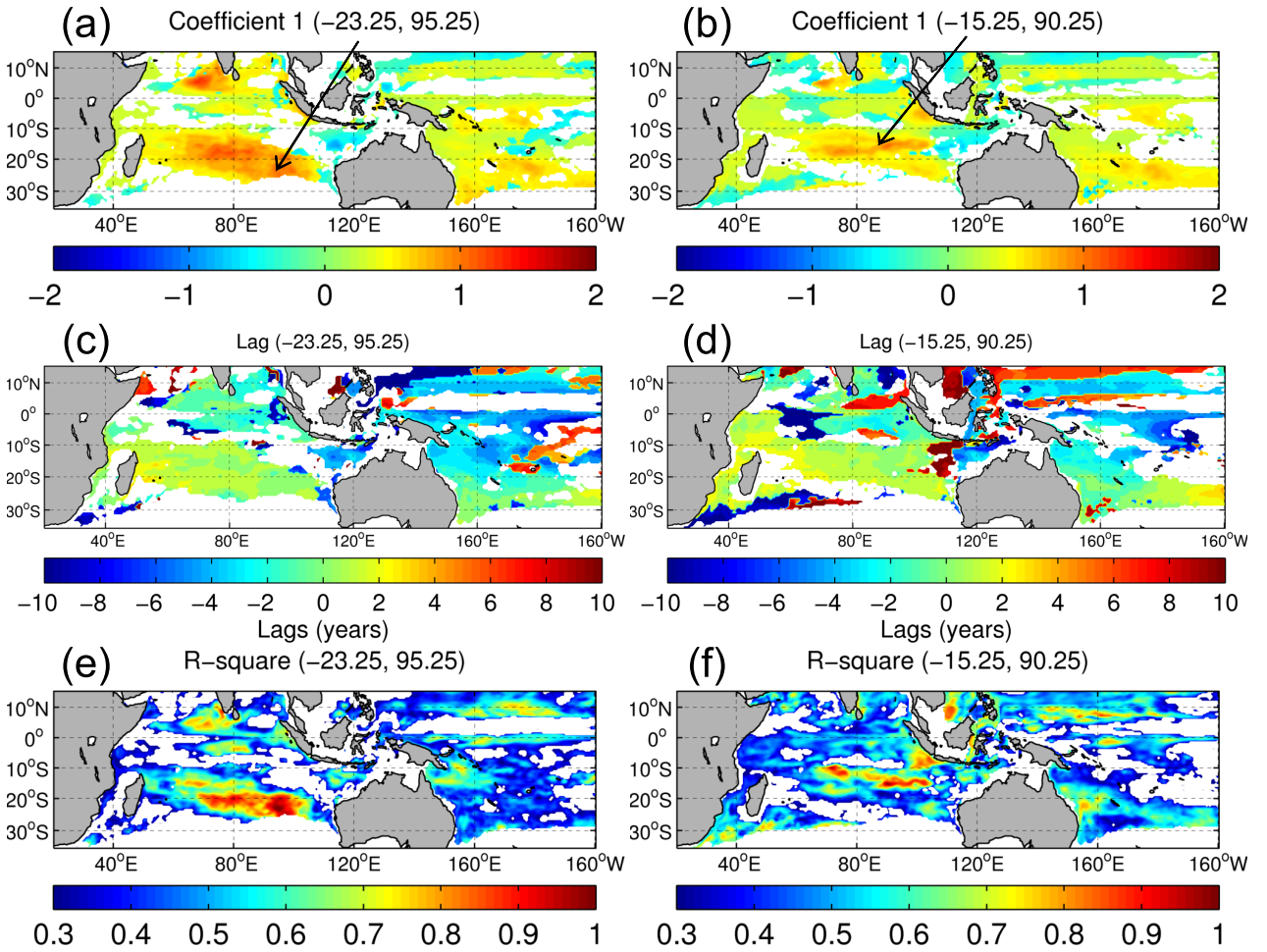

Figure 11. Lagged linear regression on salinity anomalies on D20 using as a source (predictor) a time series at (left) 23.25°S, 95.25°E and (right) 15.25°S, 90.25°E. (a, b) The regression coefficients (unitless); (c, d) the associated lags calculated every 1 year; and (e, f) the values of $R^2 \geq 0.3$ and significant at $\geq$ 95% confidence level. Detrended LP10 salinity anomalies were used. The standard deviations at sources (a) and (b) are respectively: 0.0965 and 0.1159 g kg^{-1} (std of salinity anomalies at the location of the predictor or source); 0.0245 and 0.0285 g kg^{-1} (mean of the std values of the estimates for all locations); and 0.1573 and 0.1573 (mean of the std values of the regression coefficients for all locations).

Rossby wave speeds might possibly interact with the mean flow to reduce the overall speeds of the observed anomalies [*Chang and Philander*, 1989; *Colin de Verdière and Tailleux*, 2005]. This might be possible in those regions of the tropical SPO and WTPO where there is density compensation [*Tailleux et al*., 2005].

3.10. Spatial Patterns and Sources of Salinity Anomalies Within the Thermocline

The spatial patterns of the salinity anomalies on D20 were further analyzed using a lagged linear regression (LLR) analysis to better understand the spatial connections and sources. A source (or predictor in the linear regression) located in the eastern SIO at 23.25°S, 95.25°E shows salinity anomalies on D20 being positively related to those along the central and western tropical SIO between 10°S and 25°S which appear to be independent from the anomalies along the pathway from the Indonesian Seas (Figure 11a). In contrast, a source at 15.25°S, 90.25°E, which is more influenced by the waters from the Indonesian Seas, appears to be related to the anomalies along the Makassar Strait and western tropical NPO. This pattern is unrelated to the anomalies generated further south in the SIO.

The time-lags suggest that the anomalies take 2–4 years to travel from the source locations to the western tropical SIO (Figures 11c and 11d). The statistically significant values of R^2 indicate that the LLR technique was valuable to help elucidate the connecting pathways (Figures 11e and 11f). The pattern identified by the source at 23.25°S, 95.25°E characterizes well the local contribution to the observed anomalies and matches very well with the pattern identified by the EOF analysis in Figure 3a which explains most of the variance in the region.

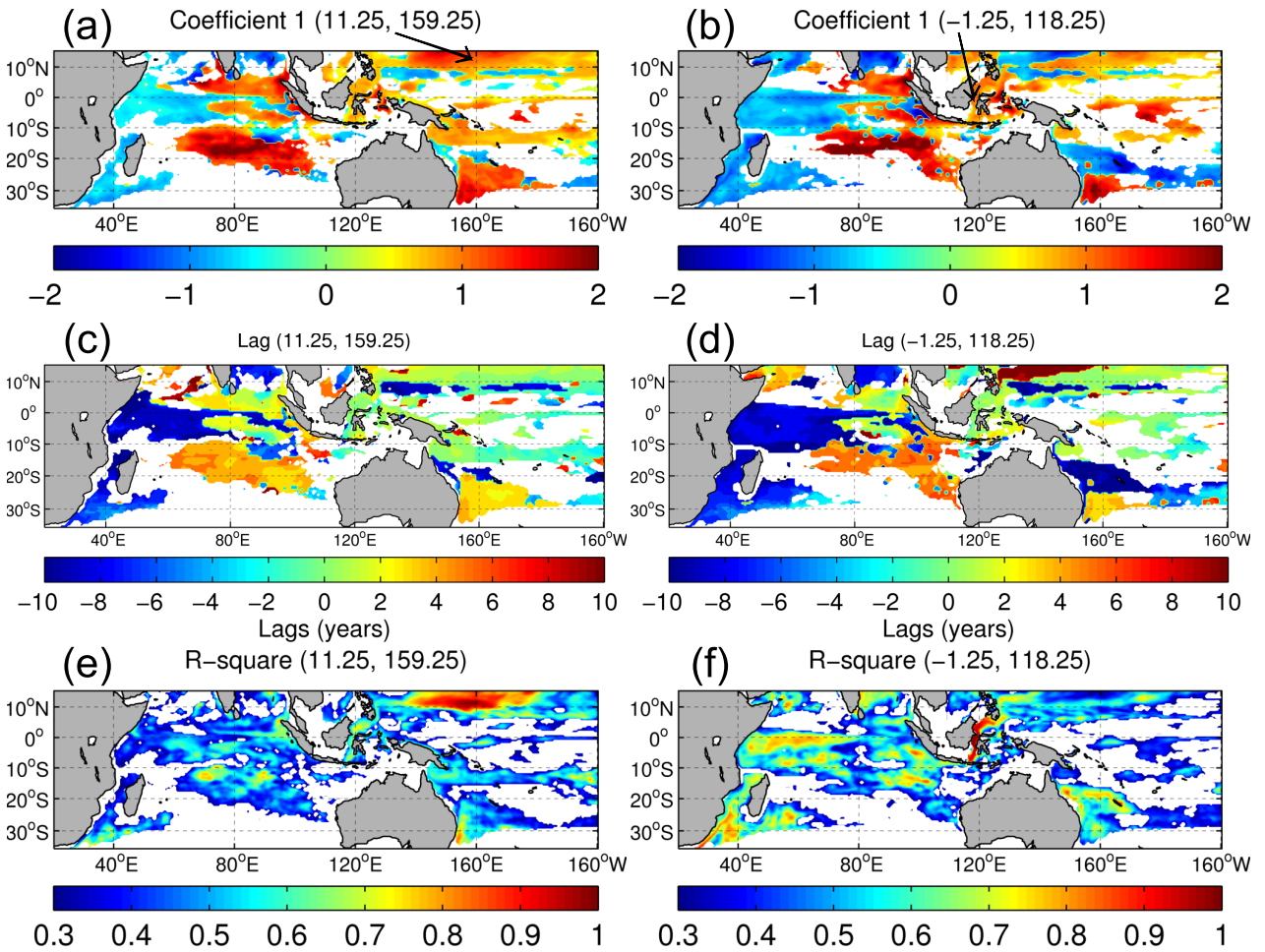

Figure 12. As Figure 11 but for the locations at 11.25°S, 159.25°E and 1.25°S, 118.25°E. The standard deviations at sources are (a) 0.0463 and (b) 0.0435 g kg^{-1} respectively: (std of salinity anomalies at the location of the predictor or source); 0.0262 and 0.0278 g kg^{-1} (mean of the std values of the estimates for all locations); and 0.3178 and 0.3912 (mean of the std values of the regression coefficients for all locations).

Two LLR analyses along the NPO-path were performed to better identify the source of anomalies originating in the western tropical NPO. The regression coefficients in the western tropical NPO and middle of Makassar Strait highlight the significant relationship of the salinity anomalies on D20 between the NPO and the tropical SIO via the NPO-path (Figures 12a and 12b). The anomalies leaving the Indonesian Seas through Lombok Strait (Figure 2) appear to split into two branches, one in the northwest direction along the Sumatra-Java coast and another leaking into the tropical SIO. The latter salinity pathway appears to connect the central tropical SIO at around 10°S, 105°E and extend to 70°E along the tropical SIO (Figure 12). Part of the anomalies east of 90°E between 15°S and 20°S travel southeastward to the WA coast (Figures 12b, 12d, and 12f). It takes around 4–6 years for the anomalies to travel from the Makassar Strait to 70°E in the tropical SIO (Figures 12c and 12d).

This remote pattern from the western tropical NPO merges with the local contribution from the SIO and intensifies the decadal signal in the tropical SIO especially around 15.25°S–20.25°S as observed in the Hovmöller plots for this zonal band (Figure 8). In addition, this pattern linked to the NPO-path contribution matches well with the pattern identified by the EOF analysis and represented by EOF5 (Figure 3i).

We performed two further LLR analyses to track the possible contribution from the western tropical SPO (not shown here for space reasons). A location offshore of Papua New Guinea at 2.75°S, 142.75°E shows a significant relationship between the salinity anomalies on D20 and the western SPO, the Indonesian Seas, Sumatra-Java coast and SIO. The SPO-path (equatorial contribution from the western SPO) and currents from further south in the western SPO supply anomalies that pass along the Papua New Guinea coast. The

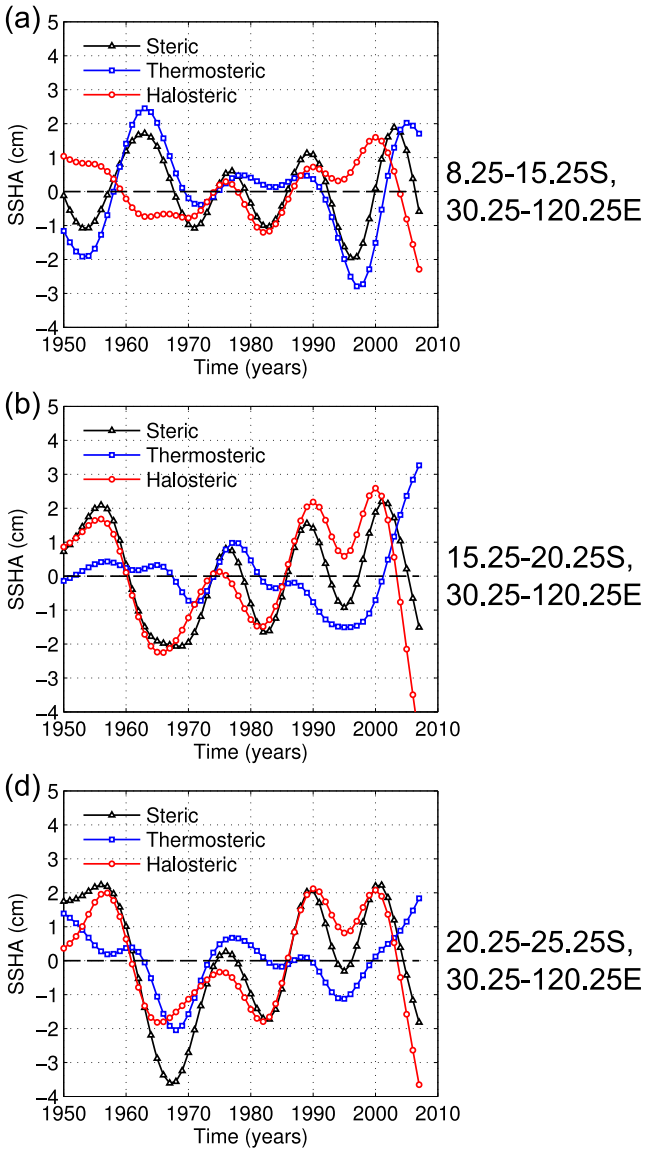

Figure 13. Steric, thermosteric and halosteric sea surface heights anomalies (upper 729 m) for three regions in the tropical SIO. Detrended 10 year low-pass Butterworth-filtered data were used.

source at 2.75°S, 142.75°E suggests also a strong covariability between the SIO and western SPO (further south of 20°S). A source at 4.25°S, 159.25°E shows the contribution from the SPO-path which appears to reach the tropical SIO via the Indonesian Seas. However, it is not completely clear from this analysis that the signal from the tropical SPO penetrates further into the tropical SIO after passing through the Indonesian Seas as there are regions in the eastern tropical SIO where R^2 is low and/or insignificant.

The strong covariability between the SIO and western SPO is evident from a LLR analysis on data further south in the western SPO at 13.25°S, 159.25°E where there are westward currents. This analysis shows that the salinity anomalies formed in the SIO are strongly related to, and in phase with, the salinity anomalies in the western SPO, specifically southward of 20°S (southward of Fiji). This strong covariability was also observed from the EOF analysis of salinity anomalies on D20 (Figure 3a). A comprehensive analysis of this covariability is beyond the scope of this paper and will be considered in a future work.

3.11. Implications for Estimates of Steric Sea Surface Heights

It was further shown that changes in salinity represent an important contribution to the steric SSHA in the tropical SIO. In the region strongly influenced by waters from the Indonesian Seas (8.25°S–15.25°S and 30.25°E–120.25°E, see box in Figure 7a) the thermosteric SSHA (only due to temperature changes) seems to be more dominant than the halosteric SSHA (only due to salinity changes) for the periods 1950–1970 and 1990–2007. However, the halosteric component dominates during the period 1970–1990, with salinity making the largest contribution to the decadal variability of steric SSHA during this time (Figure 13a).

The regions further south (15.25°S–20.25°S and 20.25°S–25.25°S, see boxes in Figures 8a and 9a respectively), which are more likely influenced by salinity anomalies from the eastern SIO, show that the decadal fluctuations of halosteric SSHA are very close to those from the steric SSHA. This means that salinity is the largest contributor to the steric SSHA decadal variability in these two regions (Figures 13b and 13c).

4. Discussion and Conclusions

This paper has examined the contribution of salinity anomalies at the depth of the thermocline from the western tropical Pacific Ocean (WTPO) and eastern South Indian Ocean (SIO) to the identified westward movement of anomalies primarily in the 8°S–20°S band of the tropical SIO on decadal-to-interdecadal (~ 10–30 years)

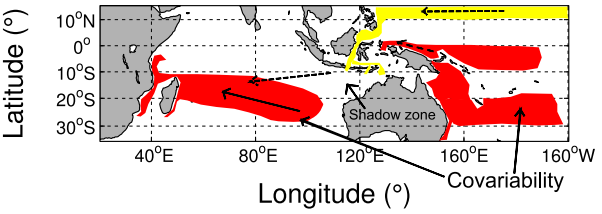

Figure 14. Schematic representation of the main sources contributing to the salinity anomaly patterns in the tropical SIO. Red colour shade (and solid arrow) in the SIO represents the contribution from the eastern SIO, yellow colour shade (and dashed arrows) represents mostly the contribution from the western tropical North Pacific Ocean via the Indonesian Seas. The contribution from the South Pacific is also depicted in red colour shade as it has strong covariability with the signal in the SIO. The penetration of this signal into the SIO was hard to track. The region off-shore North-West of Australia is related to neither of the two patters above and is named the shadow zone.

time scales for the period 1950–2007. Our analysis shows that these westward-traveling signals cannot be explained by first baroclinic-mode Rossby wave propagation or salinity advection of the mean flow from the eastern SIO, WTPO and/or Indonesian Seas. The slow speeds of the characteristic signals (0.4–1.7 cm s^{-1}) may, however, be influenced by actively advected salinity anomalies associated with nonlinear baroclinic disturbances as suggested by *O'Kane et al.* [2014] and other studies on eddy variability in the SIO [*Palastanga et al.*, 2006, 2007]. Other plausible mechanisms that can act to reduce westward travel and/or propagation speeds is by the interaction of higher baroclinic-mode wave speeds with the mean flow in density compensated regions as suggested by *Chang and Philander* [1989], *Colin de Verdière and Tailleux* [2005], and *Tailleux et al.* [2005].

O'Kane et al. [2014], using a flux-forced ocean general circulation model, have recently shown that baroclinically unstable waves can, under certain circumstances, operate in resonance with long Rossby waves and topographic steering to define characteristic pathways for these baroclinic disturbances. Our pathways in the tropical SIO reported here based on the SODA data are consistent with those described by *O'Kane et al.* [2014] in the Southern Hemisphere (see their Figure 4), and thus may provide the means to understand the physical mechanism associated with the slow westward movement of salinity anomalies in the SIO. Specifically, *O'Kane et al.* [2014] demonstrate the formation, propagation and amplification of low-frequency nonlinear disturbances of large scale within the thermocline in regions associated with Rossby wave propagation and within waveguides defined by the potential density structure. Additionally, density-compensated regions in the tropical SIO related to waters from the Indonesian Seas might allow the mean flow to interact with higher order baroclinic modes to slow down the movement of the salinity anomalies [*Chang and Philander*, 1989; *Colin de Verdière and Tailleux*, 2005; *Tailleux et al.*, 2005]. We suggest that both of these processes may contribute to explain the slow movement of the salinity anomalies observed in this study.

Regarding the sources of those salinity anomalies we find that results from a lagged linear regression (LLR) analysis agree with those from an EOF analysis in capturing the main decadal patterns of salinity anomalies at the depth of the thermocline in the SIO within the 10°S–20°S band. Those analyses suggest that the main source of the decadal salinity anomalies in that region is locally derived in the SIO and seems to follow the same path of the South Equatorial Current (SEC) along the subduction zone [see *Schott et al.*, 2009, Figure 3]. This local pattern appears in the leading EOF mode for the selected Indo-Pacific region and accounts for most of the decadal variance (39% explained by EOF1). The contribution from the western tropical Pacific Ocean and Indonesian Seas explained by EOF4/EOF5, which accounts for a combined total ~11% (EOF4 + EOF5 in Figure 3) of the variance, appears to have the largest impact on the eastern SIO even though some decadal salinity anomalies reach the central tropical SIO. Those remote salinity anomalies mostly follow the Indonesian Seas pathway and seem to join (around 90°E–100°E) those locally generated in the SIO. Part of the salinity anomalies separate from the main Indonesian Seas path, east of 100°E between 15°S and 20°S (Figures 12b, 12d, and 12f), and appear to follow the same path as the Eastern Gyral Current (EGC) [*Meyers et al.*, 1995; *Meyers*, 1996; *Domingues et al.*, 2007] as shown in the schematics by *Schott et al.* [2009, Figure 3].

In summary, we suggest that there may be three sources that influence the westward-moving salinity anomalies in the tropical SIO: the eastern subtropical SIO, the western tropical NPO and the western tropical SPO (Figure 14). The locally derived and remote patterns join in the central tropical SIO along the zonal band 8.25°S–15.25°S (Figure 14). The schematics in Figure 14 agree with the paths of ventilated zones in the SIO. The branch extending from the eastern to western SIO corresponds well with the thermocline-ventilated trajectories reported by *Harper* [2000] using a high-resolution global circulation model and also it follows the same SEC path along the subduction zone [*Schott et al.*, 2009] as already mentioned. This

pathway also matches one of the "storm tracks" of baroclinic disturbances found by *O'Kane et al*. [2014]. The tropical western NPO seems to supply more remote salinity anomalies into the tropical SIO than the western SPO as the signal from the latter is more difficult to track due to the strong mixing in the Banda Sea. It is likely that the final contribution from the WTPO into the tropical SIO is a mix between the two sources from the NPO and SPO. Finally, variability in the northwest of Australia is defined by a very different spatial pattern and decadal time signature than elsewhere (Figure 14). This region seems to match with the unventilated area of the eastern tropical SIO that has low levels of oxygen and is known in the literature as the "shadow zone."

Results from the present study suggest that the signals of salinity anomalies on D20 from the western tropical North Pacific Ocean and the western tropical South Pacific Ocean vary on decadal-to-interdecadal time scales (from 10 to 30 years, respectively). The mean flow paths (NPO-path and SPO-path) shown in this study agree very well with the pathways identified by *Gordon and Fine* [1996], *Wijffels et al*. [2008], *Tillinger* [2011], and *Valsala et al*. [2010, 2011] while the salinity anomaly pathways in the SIO being consistent with those recently reported in terms of nonlinear baroclinic disturbances [*O'Kane et al*., 2014] and not necessarily following the mean flow paths. The salinity anomaly signals from the western tropical Pacific Ocean could be the low-frequency response of the salinity variability found by *Valsala et al*. [2011] who explain that shallower waters from the western tropical North Pacific Ocean feed the Indonesian Seas on interannual time scales whereas deeper waters from the western tropical-equatorial South Pacific Ocean feed the Indonesian Seas on interdecadal time scales.

The eastern tropical SIO, mostly within the 8.25°–15.25°S band, is dominated by interdecadal signals with westward speeds of around 0.4 cm s^{-1} likely from the western tropical Pacific Ocean. The western and central tropical SIO (8.25°–15.25°S) are mostly dominated by decadal signals with westward speeds of around 1.7 cm s^{-1}. The central tropical SIO is influenced by both remote and local salinity anomalies whereas the western tropical SIO is mostly dominated by decadal signals generated further south in the eastern SIO (20°S–30°S) that have also been detected in SST, SSH and D20 anomalies by *Trenary and Han* [2013].

The difficulty of tracking the movement of salinity anomalies in some regions using the lagged linear regression technique, in particular from the western tropical South Pacific Ocean into the Indonesian Seas and hence into the eastern tropical SIO, may be related to the strong mixing in the Indonesian Seas associated with high tidal energy which contributes to the strong transformation of Pacific water masses within the Indonesian archipelago, as proposed by *Koch-Larrouy et al*. [2007]. Interestingly, it was possible to track the movement of salinity anomalies from the western tropical North Pacific Ocean into the tropical SIO, despite the narrow straits (e.g., Makassar Strait) having stronger mixing and water mass transformation than other regions, like in the Banda Sea [*Koch-Larrouy et al*., 2007]. This potentially reduced signal from the western tropical Pacific Ocean converges with the locally derived stronger signal in the eastern tropical SIO, after which they travel westward across the tropical SIO.

This study has also shown that decadal variability of SSHA within the 8.25°S–15.25°S band of the tropical SIO is dominated by thermosteric changes likely albeit in combination with the fresher waters from the Indonesian Seas. Conversely, further south in the SIO (15.25°S–25.25°S) decadal variability of SSHA is halosteric dominated due to the influence of the saltier waters from the eastern SIO. This finding demonstrates the importance of understanding the decadal variability and movement of salinity anomalies to describe better the long-term sea level changes in the Indian Ocean.

The strong covariability between the salinity anomaly pattern in the SIO (what it is considered here to be the local contribution from the eastern SIO) and the western SPO suggests that these two regions are strongly related and exhibit decadal variability nearly in phase. Since the salinity anomaly patterns appear to be almost in phase, this suggests that the strong positive relationship could be induced by westerly winds from the Southern Ocean, as the salinity anomalies are significantly anticorrelated with the Southern Annular Mode index (not shown here). A detailed analysis of this covariability is beyond the scope of this paper and will instead be considered in future research.

The conclusions drawn in this paper are as follows: (1) the study has shown a decadal signal in salinity anomalies on the depth of the 20°C isotherm (a proxy for the depth of the thermocline) in the tropical SIO (8°S–20°S) that is unlikely to be due either to linear first-baroclinic mode Rossby wave propagation or salinity advection by the mean flow in isolation. Instead, the slow westward travel times of the salinity anomalies

in the tropical SIO may also be due, at least in part, to self-advected anomalies that involve nonlinear baroclinic disturbances as proposed by *O'Kane et al.* [2014] and/or interaction of higher order baroclinic modes with the mean flow as theorized by *Chang and Philander* [1989], *Colin de Verdière and Tailleux* [2005], and *Tailleux et al.* [2005]. (2) The identified salinity anomaly signal is mostly locally derived by salinity anomalies from the eastern SIO which merge with remote anomalies from the western tropical Pacific Ocean and Indonesian Seas. However, the latter explains a lower (but nevertheless significant) amount of the variance in the SIO. 3) Decadal variability of salinity anomalies from the western tropical South Pacific Ocean has a deeper vertical expression than those from the western tropical North Pacific Ocean. 4) The slow westward-traveling salinity anomalies are at least partly responsible for the associated steric SSH changes in the tropical SIO.

Acknowledgments

This work was conducted as part of the José Mauro Vargas Hernández PhD in Quantitative Marine Sciences (QMS) Ph.D. Program, a joint initiative between the University of Tasmania and CSIRO. This research was partially supported by grants from the QMS PhD Scholarship, Postgraduate Studies Scholarship from Universidad Nacional of Costa Rica and CSIRO Wealth from Oceans Flagship Scholarship. SODA 2.2.4 data are provided by SODA/TAMU research group, Texas A&M University, available at the web site http://soda.tamu.edu/. Vertical profiles of potential temperature in degrees Celcius (°C), salinity in pratical salinity units (PSU) and depth in metres (m) at two locations from CARS were provided by Dr. Jeff Dunn from CSIRO Marine and Atmospheric Research (also available at www.cmar.csiro.au/cars). The IPO index was obtained from the calculations of Chris Folland, UK Met Office Hadley Centre at http://www.iges.org/c20c/IPO_v2.doc. This paper makes a contribution to the goals of the Australian Research Council Centre of Excellence for Climate System Science and the Australian Climate Change Science Program.

References

Alory, G., and G. Meyers (2009), Warming of the upper Equatorial Indian Ocean and changes in the heat budget (1960-99), *J. Clim.*, *22*(1), 93–113, doi:10.1175/2008JCLI2330.1.

Alory, G., S. Wijffels, and G. Meyers (2007), Observed temperature trends in the Indian Ocean over 1960–1999 and associated mechanisms, *Geophys. Res. Lett.*, *34*, L02606, doi:10.1029/2006GL028044.

Cai, W., G. Meyers and G. Shi (2005), Transmission of ENSO signal to the Indian Ocean, *Geophys. Res. Lett.*, *32*, L05616, doi:10.1029/2004GL021736.

Cai, W., A. Sullivan, and T. Cowan (2008), Shoaling of the off-equatorial south Indian Ocean thermocline: Is it driven by anthropogenic forcing?, *Geophys. Res. Lett.*, *35*, L12711, doi:10.1029/2008GL034174.

Carton, J., and B. Giese (2008), A reanalysis of ocean climate using Simple Ocean Data Assimilation (SODA), *Mon. Weather Rev.*, *136*(8), 2999–3017, doi:10.1175/2007MWR1978.1.

Challenor, P. G., P. Cipollini, and D. Cromwell (2001), Use of the 3D Radon transform to examine the properties of oceanic Rossby waves, *J. Atmos. Oceanic Technol.*, *18*(9), 1558–1566, doi:10.1175/1520-0426(2001)018<1558:UOTRTT>2.0.CO;2.

Chang, P., and S. Philander (1989), Rossby wave packets in baroclinic mean currents, *Deep Sea Res., Part A*, *36*(1), 17–37.

Chelton, D. B., R. A. DeSzoeke, M. G. Schlax, K. El Naggar, and N. Siwertz (1998), Geographical variability of the first baroclinic Rossby radius of deformation, *J. Phys. Oceanogr.*, *28*(3), 433–460, doi:10.1175/1520-0485(1998)028<0433:GVOTFB>2.0.CO;2.

Colin de Verdière, A., and R. Tailleux (2005), The interaction of a baroclinic mean flow with long Rossby waves, *J. Phys. Oceanogr.*, *35*(5), 865–879, doi:10.1175/JPO2712.1.

Domingues, C. M., M. E. Maltrud, S. E. Wijffels, J. A. Church, and M. Tomczak (2007), Simulated Lagrangian pathways between the Leeuwin Current System and the upper-ocean circulation of the southeast Indian Ocean, *Deep Sea Res., Part II*, *54*(8), 797–817, doi:10.1016/j.dsr2.2006.10.003.

Feng, M., Y. Li, and G. Meyers (2004), Multidecadal variations of Fremantle sea level: Footprint of climate variability in the tropical Pacific, *Geophys. Res. Lett.*, *31*, L16302, doi:10.1029/2004GL019947.

Feng, M., M. McPhaden, and T. Lee (2010), Decadal variability of the Pacific subtropical cells and their influence on the southeast Indian Ocean, *Geophys. Res. Lett.*, *37*, L09606, doi:10.1029/2010GL042796.

Feng, M., C. Böning, A. Biastoch, E. Behrens, E. Weller, and Y. Masumoto (2011), The reversal of the multi-decadal trends of the equatorial Pacific easterly winds, and the Indonesian Throughflow and Leeuwin Current transports, *Geophys. Res. Lett.*, *38*, L11604, doi:10.1029/2011GL047291.

Gill, A. E. (1982), *Atmosphere-Ocean Dynamics*, vol. 30, 662 pp., Academic, N. Y.

Gordon, A. L., and R. A. Fine (1996), Pathways of water between the Pacific and Indian oceans in the Indonesian seas, *Nature*, *379*(6561), 146–149.

Han, W., G. A. Meehl, and A. Hu (2006), Interpretation of tropical thermocline cooling in the Indian and Pacific oceans during recent decades, *Geophys. Res. Lett.*, *33*, L23615, doi:10.1029/2006GL027982.

Han, W., et al. (2010), Patterns of Indian Ocean sea-level change in a warming climate, *Nat. Geosci.*, *3*(8), 546–550, doi:10.1038/ngeo901.

Han, W., J. Vialard, M. J. McPhaden, T. Lee, Y. Masumoto, M. Feng, and W. P. de Ruijter (2014), Indian Ocean decadal variability: A review, *Bull. Am. Meteorol. Soc.*, doi:10.1175/BAMS-D-13-00028.1.

Harper, S. (2000), Thermocline ventilation and pathways of tropical–subtropical water mass exchange, *Tellus, Ser. A*, *52*(3), 330–345, doi:10.1034/j.1600-0870.2000.d01-7.x.

Hirst, A. C., and J. Godfrey (1993), The role of Indonesian throughflow in a global ocean GCM, *J. Phys. Oceanogr.*, *23*(6), 1057–1086, doi:10.1175/1520-0485(1993)023<1057:TROITI >2.0.CO;2.

Koch-Larrouy, A., G. Madec, P. Bouruet-Aubertot, T. Gerkema, L. Bessières, and R. Molcard (2007), On the transformation of Pacific Water into Indonesian Throughflow Water by internal tidal mixing, *Geophys. Res. Lett.*, *34*, L04604, doi:10.1029/2006GL028405.

Kundu, P. K., and J. P. McCreary Jr (1986), On the dynamics of the throughflow from the Pacific into the Indian Ocean, *J. Phys. Oceanogr.*, *16*(12), 2191–2198, doi:10.1175/1520-0485(1986)016<2191:OTDOTT>2.0.CO;2.

Lee, T., and M. J. McPhaden (2008), Decadal phase change in large-scale sea level and winds in the Indo-Pacific region at the end of the 20th century, *Geophys. Res. Lett.*, *35*, L01605, doi:10.1029/2007GL032419.

Maharaj, A., N. Holbrook, and P. Cipollini (2009), Multiple westward propagating signals in South Pacific sea level anomalies, *J. Geophys. Res.*, *114*, C12016, doi:10.1029/2008JC004799.

Meyers, G. (1996), Variation of Indonesian throughflow and the El Niño-Southern Oscillation, *J. Geophys. Res.*, *101*(C5), 12,255–12,263, doi:10.1029/95JC03729.

Meyers, G., R. Bailey and A. Worby (1995), Geostrophic transport of Indonesian throughflow, *Deep Sea Res., Part I*, *42*(7), 1163–1174, doi:10.1016/0967-0637(95)00037-7.

Nidheesh, A. G., M. Lengaigne, J. Vialard, A. S. Unnikrishnan, and H. Dayan (2013), Decadal and long-term sea level variability in the tropical Indo-Pacific Ocean, *Clim. Dyn.*, *41*(2), 381–402, doi:10.1007/s00382-012-1463-4.

North, G. R., T. L. Bell, R. F. Cahalan, and F. J. Moeng (1982), Sampling errors in the estimation of empirical orthogonal functions, *Mon. Weather Rev.*, *110*(7), 699–706, doi:10.1175/1520-0493(1982)110<0699:SEITEO>2.0.CO;2.

O'Kane, T., R. Matear, M. Chamberlain, E. Oliver, and N. Holbrook (2014), Storm tracks in the southern hemisphere subtropical oceans, *J. Geophys. Res. Oceans*, *119*, 6078–6100, doi:10.1002/2014JC009990.
Palastanga, V., P. Van Leeuwen, and W. De Ruijter (2006), A link between low-frequency mesoscale eddy variability around Madagascar and the large-scale Indian Ocean variability, *J. Geophys. Res.*, *111*, C09029, doi:10.1029/2005JC003081.
Palastanga, V., P. Van Leeuwen, M. Schouten, and W. De Ruijter (2007), Flow structure and variability in the subtropical Indian Ocean: Instability of the South Indian Ocean Countercurrent, *J. Geophys. Res.*, *112*, C01001, doi:10.1029/2005JC003395.
Reason, C., R. Allan, and J. Lindesay (1996), Evidence for the influence of remote forcing on interdecadal variability in the southern Indian Ocean, *J. Geophys. Res.*, *101*(C5), 11,867–11,882, doi:10.1029/96JC00122.
Ridgway, K., J. Dunn, and J. Wilkin (2002), Ocean interpolation by four-dimensional weighted least squares-application to the waters around Australasia, *J. Atmos. Oceanic Technol*, *19*(9), 1357–1375, doi:10.1175/1520-0426(2002)019¡1357:OIBFDW¿2.0.CO;2.
Schoenefeldt, R., and F. A. Schott (2006), Decadal variability of the Indian Ocean cross-equatorial exchange in SODA, *Geophys. Res. Lett.*, *33*, L08602, doi:10.1029/2006GL025891.
Schott, F. A., S.-P. Xie, and J. P. McCreary (2009), Indian Ocean circulation and climate variability, *Rev. Geophys.*, *47*, RG1002, doi:10.1029/2007RG000245.
Schwarzkopf, F. U., and C. W. Böning (2011), Contribution of Pacific wind stress to multi-decadal variations in upper-ocean heat content and sea level in the tropical south Indian Ocean, *Geophys. Res. Lett.*, *38*, L12602, doi:10.1029/2011GL047651.
Shi, G., J. Ribbe, W. Cai, and T. Cowan (2007), Multidecadal variability in the transmission of ENSO signals to the Indian Ocean, *Geophys. Res. Lett.*, *34*, L09706, doi:10.1029/2007GL029528.
Tailleux, R., A. Lazar, and C. Reason (2005), Physics and dynamics of density-compensated temperature and salinity anomalies. Part I: Theory, *J. Phys. Oceanogr.*, *35*(5), 849–864, doi:10.1175/JPO2706.1.
Tillinger, D. (2011), Physical oceanography of the present day Indonesian Throughflow, *Geol. Soc. Spec. Publ.*, *355*(1), 267–281, doi:10.1144/SP355.13.
Timmermann, A., S. McGregor, and F.-F. Jin (2010), Wind effects on past and future regional Sea level trends in the Southern Indo-Pacific, *J. Clim.*, *23*(16), 4429–4437, doi:10.1175/2010JCLI3519.1.
Trenary, L., and W. Han (2008), Causes of decadal subsurface cooling in the tropical Indian Ocean during 1961–2000, *Geophys. Res. Lett.*, *35*, L17602, doi:10.1029/2008GL034687.
Trenary, L. L., and W. Han (2013), Local and remote forcing of decadal sea level and thermocline depth variability in the South Indian Ocean, *J. Geophys. Res. Oceans*, *118*, 381–398, doi:10.1029/2012JC008317.
Valsala, V., S. Maksyutov, and R. Murtugudde (2010), Possible interannual to interdecadal variabilities of the Indonesian throughflow water pathways in the Indian Ocean, *J. Geophys. Res.*, *115*, C10016, doi:10.1029/2009JC005735.
Valsala, V., S. Maksyutov, and R. Murtugudde (2011), Interannual to Interdecadal variabilities of the Indonesian Throughflow source water pathways in the Pacific Ocean, *J. Phys. Oceanogr.*, *41*(10), 1921–1940, doi:10.1175/2011JPO4561.1.
Vargas-Hernández, J. M. (2014), Decadal climate variability in the Indo-Pacific upper ocean from state estimates, PhD thesis, Univ. of Tas., Hobart, Australia.
Vargas-Hernandez, J. M., S. Wijffels, G. Meyers and N. J. Holbrook (2014), Evaluating SODA for Indo-Pacific Ocean decadal climate variability studies, *J. Geophys. Res. Oceans*, *119*, 7854–7868, doi:10.1002/2014JC010175.
Venegas, S. A. (2001), Statistical methods for signal detection in climate, *Dan. Cent. Earth Syst. Sci. Rep.*, *2*, 96.
Wainwright, L., G. Meyers, S. Wijffels and L. Pigot (2008), Change in the Indonesian Throughflow with the climatic shift of 1976/77, *Geophys. Res. Lett.*, *35*, L03604, doi:10.1029/2007GL031911.
Wijffels, S., and G. Meyers (2004), An intersection of oceanic waveguides: Variability in the Indonesian throughflow region, *J. Phys. Oceanogr.*, *34*(5), 1232–1253.
Wijffels, S. E., G. Meyers and J. S. Godfrey (2008), A 20-yr average of the Indonesian Throughflow: Regional currents and the interbasin exchange, *J. Phys. Oceanogr.*, *38*(9), 1965–1978, doi:10.1175/2008JPO3987.1.
Zhang, X., and J. A. Church (2012), Sea level trends, interannual and decadal variability in the Pacific Ocean, *Geophys. Res. Lett.*, *39*, L21701, doi:10.1029/2012GL053240.